Dynamics of Drop Impact on Solid Surface: Experiments and VOF Simulations

Prashant R. Gunjal, Vivek V. Ranade, and Raghunath V. Chaudhari
Industrial Flow Modeling Group, Homogeneous Catalysis Division, National Chemical Laboratory, Pune 411008, India

DOI 10.1002/aic.10300
Published online in Wiley InterScience (www.interscience.wiley.com).

The process of spreading/recoiling of a liquid drop after collision with a flat solid surface was experimentally and computationally studied to identify the key issues in spreading of a liquid drop on a solid surface. The long-term objective of this study is to gain an insight in the phenomenon of wetting of solid particles in the trickle-bed reactors. Interaction of a falling liquid drop with a solid surface (impact, spreading, recoiling, and bouncing) was studied using a high-speed digital camera. Experimental data on dynamics of a drop impact on flat surfaces (glass and Teflon) are reported over a range of Reynolds numbers (550–2500) and Weber numbers (2–20). A computational fluid dynamics (CFD) model, based on the volume of fluid (VOF) approach, was used to simulate drop dynamics on the flat surfaces. The experimental results were compared with the CFD simulations. Simulations showed reasonably good agreement with the experimental data. A VOF-based computational model was able to capture key features of the interaction of a liquid drop with solid surfaces. The CFD simulations provide information about finer details of drop interaction with the solid surface. Information about gas–liquid and liquid–solid drag obtained from VOF simulations would be useful for CFD modeling of trickle-bed reactors.
 AIChE J, 51: 59–78, 2005
Keywords: drop impact, spreading, recoiling, VOF, CFD, trickle bed

Introduction

Interaction of liquid drops with solid surfaces occurs in a variety of processes ranging from spray coating, drying, and cooling to wetting of packings or catalyst pellets. The present study is motivated by the necessity to learn more about the fundamental processes in wetting of catalyst pellets in trickle-bed reactors. In trickle-bed reactors (TBR), gas and liquid phases flow cocurrently downward through the packed bed (of catalyst pellets). Two-phase frictional pressure drop, liquid holdup, and degree of wetting are some of the key and essential parameters for designing of these reactors. Wetting of catalyst particles directly affects the use of the catalyst bed and the performance of the trickle-bed reactors. Measurements of degree of wetting in a packed bed reactor are rather difficult and require sophisticated techniques such as MRI (magnetic resonance imaging; see Gladden, 2003). These techniques give detailed 3-D gas–liquid distribution along with flow field information with a high spatial resolution. The applicability of such techniques is still in a developing stage. Developments in theoretical models and their numerical solution are essential to make practical use of these data.

In recent years, computational fluid dynamics (CFD)–based models are used to understand the complex hydrodynamics of TBR (see, for example, Gunjal et al., 2003; Jiang et al., 2002). Such CFD models may provide better understanding of liquid distribution and wetting phenomena in trickle-bed reactors. However, presently available CFD models (based on the Eulerian–Eulerian approach) are unable to capture the observed hysteresis in the operation of trickle beds (Gunjal et al., 2003). The hysteresis observed in the trickle beds (of pressure drop, liquid saturation, and so on) is directly related to the spreading of a liquid on either wet or dry solid surfaces. It is therefore important to understand spreading of liquid on the solid sur-

Correspondence concerning this article should be addressed to V. V. Ranade at vvranade@ifmg.ncl.res.in.

Table 1. Summary of the Previous Work Done on Impact of Drop in Solid Surface

	Authors	Objective of Work	Scope of Work	Impact Velocity (m/s)	Contact Angle (°)	Re	We	Method
1	Fukai et al. (1995)	Drop oscillation	2-D model development	1–3.76	30–150	1500–4500	37–530	2-D Lagrangian grid model
2	Scheller et al. (1995)	Maximum spread	Wide range of viscosities ~ 300 Pa · s	1.4–4.9	35–90	19–16,400	56–364	Experimental and empirical
3	Pasandideh-Fard et al. (1996)	Effect of surfactant	Experimental as well as numerical study	1	20–85	2000	27–40	Experimental and SOLA-VOF model
4	Mao et al. (1997)	Maximum spread and rebound criteria	Drop spreading, rebounding and splashing, and equilibrium diameter	0.5–6.0	45–95	1490–10,000	11–518	Experiments and analytical
5	Zhang and Basaran (1997)	Effect of surfactant on drop dynamics	Experimental study: lower and higher concentration of surfactant	0.5–1	>54	1040–13,000	440–1300	Experimental investigation
4	Bussmann et al. (1999)	Drop flow on inclined surface and edge	Drop solidification	1–1.2	60–90	2000–2400	27	Experimental and VOF model
5	Davidson (2000)	Applicability of the BEM for inviscid drop spreading	Drop height and spreading	1–3	90	200–300	2–50	Boundary integral method
6	Bussmann et al. (2000)	Splashing study of droplet	Model for splashing and effect of various parameters on splashing	1–4	32–148*	9000–28,000	36–1060	Experimental and VOF model
7	Crooks et al. (2001)	Role of elasticity on dynamics of drop	Spreading, rebounding	1–3	6–108	—	—	Experimental
8	Richard et al. (2002)	Bouncing drop	Contact time with surface	0.5–2.5	Hydrophobic surface	20–4600	3–144	Experimental
9	Pasandideh-Fard et al. (2002)	Solidification of drop on impact	Spread factor during solidification on flat and inclined surface	1	60–90	—	—	VOF solidification simulations
10	Reznik and Yarin (2002)	Theoretical study	Viscous drop spreading	0.1–1	<180	0.001–1	1–500	Analytical method
11	This study	Fluid dynamics and numerical issues	Spreading, rebounding, splashing, bouncing drop	0.22–4	45–179	550–1E5	2–1350	Experimental and VOF model

*Dynamic contact angle.

faces (see, for example, Gunjal et al., 2003; Liu et al., 2002; Szady and Sundaresan, 1991) for making further progress in understanding operation of trickle beds. To understand the wetting phenomenon, it is essential to formulate detailed CFD models that can capture the microscale interaction processes of liquid and solid surfaces. Such an attempt is made in this work. The focus was on developing computational models for simulating free surface flows and using these computational models to gain insight and quantitative information about the process of interaction of a liquid drop with the solid surfaces. It is important to carry out experiments to guide the development and to evaluate the computational models.

In the present work, a case of an interaction of a single liquid drop with a flat solid surface was selected as a model problem. To understand the effect of various parameters such as liquid velocity, surface tension, and wetting, experiments were carried out over a wide range of operating conditions relevant to operation of trickle-bed reactors. The process of spreading/recoiling of a liquid drop after impact on a flat solid surface was experimentally and computationally studied to identify key issues in spreading of a liquid drop on solid surface. Before discussing the present work, previous studies are briefly reviewed in the following subsection.

Previous work

The phenomenon of a drop impact with the solid surface has been extensively studied because of its widespread applications (see, for example, Bergeron et al., 2000; Chandra and Avedisian, 1991, 1992; Crookes et al., 2001; de Gennes, 1985; Fukai et al., 1993, 1995; Mao et al., 1997; Richard et al., 2002; Rioboo et al., 2002; Scheller and Bousfield, 1995; Stow and Hadfield, 1981; Zhang and Basaran, 1997 and reference cited therein). Scheller and Bousfield (1995) studied drop spreading on polystyrene and glass surfaces for a wide range of liquid properties (viscosity 1–300 mPa·s and surface tension 65–72 mN/m). The maximum spread diameter was correlated as a function of the Reynolds (Re) and Ohnesorge (Oh) numbers. Mao et al. (1997) experimentally studied drop spreading and rebounding phenomenon at different values of contact angle (CA) and impact velocity. They reported experimental data on the maximum spread diameter for different impact velocities. Richard et al. (2002) reported the contact time of droplets bouncing on a nonwetted solid surface at various impacting velocities and drop diameters. Previous experimental studies and parameter ranges considered in these studies are summarized in Table 1. It may be noted that most of the previous

studies were restricted to higher-impact velocities (>1 m/s). Very few experimental studies and simulations were carried out with lower (<1 m/s) impact velocities. Most of these studies were carried out at high Reynolds number (Re < 1000) and Weber numbers (We < 20). Unlike the ranges considered in the previous studies, interaction of liquid drops with solid surfaces occurs at much lower velocities in the trickle-bed reactors (~0.05–1.0 m/s). Contact angle variation, physical properties of liquid drop variation (in terms of dimensionless numbers Re and We or Oh), and purpose of their study are summarized in Table 1. Additional experimental investigations for the ranges relevant to the trickle-bed reactor are thus needed.

Interaction of a surfactant containing a liquid drop with the solid surface might be very different from that of a drop without containing the surfactant. Several studies have been carried out to understand the influence of a surfactant on the dynamics of drop impact with a solid surface (for example, Crooks et al., 2001; Mourougou-Candoni et al., 1997; Pasandideh-Fard et al., 1996; Thoroddsen and Sakakibara, 1998; Zhang and Basaran, 1997). If the characteristic timescale of surfactant diffusion within the drop is larger than or comparable to the characteristic timescale of spreading/recoiling, surfactant concentration within the drop may become spatially nonhomogeneous. In such a case, the impact dynamics of the drop was found to be very different. The study by Zhang and Basaran (1997) suggested that for the relatively low molecular weight surfactants such as sodium dodecyl sulfate (SDS), surfactant transport rates are fast enough to ensure that surfactant concentration remains uniform within the drop during the impact process (even up to impact velocities of 2 m/s). Thus, studies of the drop impact process with addition of surfactants such as SDS might be useful to isolate and to understand the influence of surface tension on the drop impact process without complications of variation of surfactant concentration within the drop.

Most of the previous modeling work was focused on developing either empirical or theoretical models to predict maximum spread and/or criterion for rebound (Crooks et al., 2001; Mao et al., 1997). Although such models provide some insight into drop interaction with solids, they are unable to provide detailed information such as: interactions of gas and liquid phases, variation of drop surface area, solid–liquid contact area, and velocity field within the drop with time. Such information is needed to gain detailed insight into wetting and macroscopic closure models used in trickle-bed reactor models. Various computational approaches have been used to simulate free surface flows such as drop impact. They are briefly reviewed in the section describing the present computational model. Here, some of the simulation studies are reviewed briefly.

Fukai et al. (1995) used an adaptive finite-element method to simulate the impact of a drop on a flat surface. Experiments as well as simulation results were shown at various operating conditions. For this study, impact velocities were in the range of 1–2 m/s. They found that incorporation of advancing and receding angles in the model improves the results. Pasandideh-Fard et al. (1996) carried out simulations of impact of a drop using a modified solution algorithm–volume of fluid (SOLA-VOF) method. In this study, drop contact angle variation was considered during each time step and simulated results were compared with their experimental data of drop spreading. Bussmann et al. (2000) studied drop splashing with experiments as well as simulations. Average values of dynamic contact angle measured from experiments were used for simulation and splashing was studied at high impact velocity (>1.5 m/s). Davidson (2000, 2002) used a boundary integral method to study deformation of a drop on a flat surface. In his study, applicability of the boundary integral method for an inviscid drop deformation was assessed for different values of Weber number (5–25). A linear viscous term was derived from this study to understand the role of viscosity on drop deformation. Recently Pasandideh-Fard et al. (2002) studied solidification of the molten drop on flat and inclined surfaces with an interface tracking algorithm and continuum surface force (CSF) model in a three-dimensional (3D) domain.

Most of the previous modeling attempts were restricted in their simulations to the initial period of the drop impact, usually covering just the first cycle of spread and recoil (simulations were carried out for time less than about 50 ms). Systematic studies covering several cycles of spread and recoil are needed to evaluate whether CFD models capture the overall dynamics correctly. Such validated models may then be used to gain better insight into the drop flow field under spreading/recoiling over solid surfaces.

Present contribution

The present work was undertaken to develop CFD models to simulate drop impact on a solid surface with lower impact velocities and to provide experimental data to evaluate CFD models. A high-speed camera was used to characterize the drop impact by measuring drop oscillation periods and spreading and recoiling velocities. Experiments were performed at various impact velocities (0.22–4 m/s) for systems covering a wide range of contact angles (40–180°). Two different surfaces (glass and Teflon) and two liquids, water (with or without surfactant) and mercury, were used to achieve different drop interaction regimes. Experiments were carried out for the following three distinct regimes of drop interaction with flat surfaces:

(1) *Oscillations*: drop spreads and recoils many times before coming to the rest

(2) *Rebounding*: drop bounces from the surface

(3) *Splashing*: drop breaks into smaller droplets

Static and dynamics contact angles were obtained from the experimental data. A VOF-based model was used to simulate the drop impact phenomenon. Surface tension and wall adhesion phenomena were taken into account in this model. The influences of several parameters such as drop diameter, liquid surface tension, and solid surface properties were studied with the help of experiments as well as simulations. The drop oscillation period, rebounding, and wall adhesion were studied. Simulated results of drop height variation were compared with the experimental data. From validated simulations, variations of interfacial area and solid–liquid contacting area during the oscillatory phase were obtained. The detailed flow field information was found to be useful for calculating gas–liquid and liquid–solid interaction in terms of average shear stress acting at the corresponding interfaces. The reported results and further extensions of the present work have potentially significant implications for CFD modeling of trickle-bed reactors.

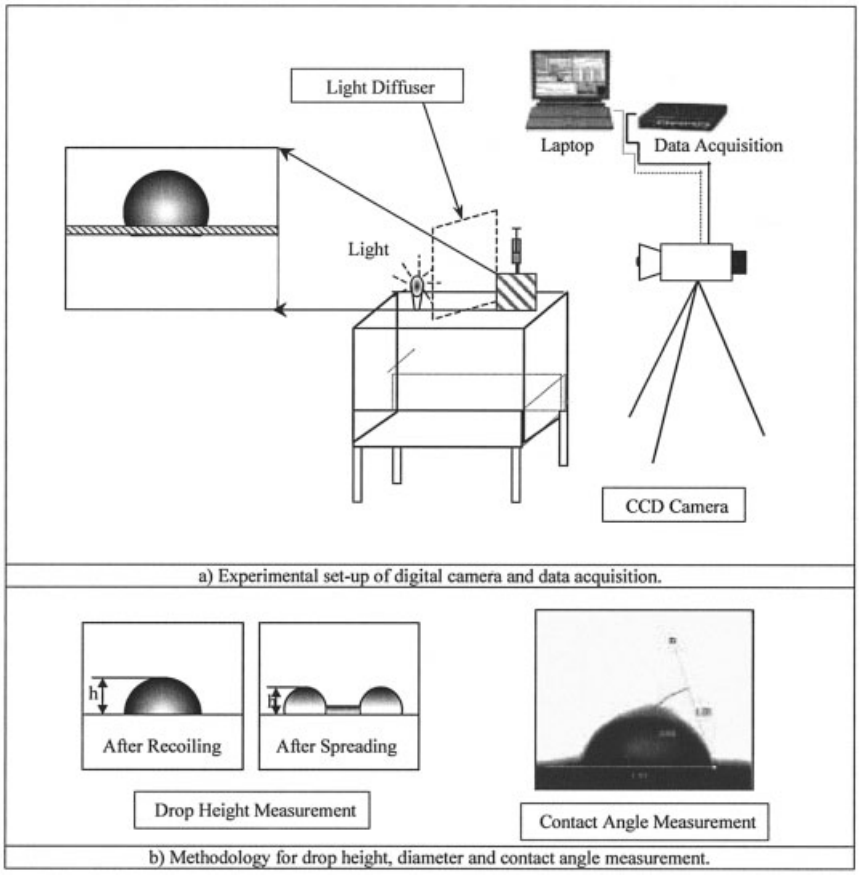

Figure 1. Experimental setup for studying drop dynamics with high-speed digital camera.

Experimental Setup and Procedure

The experimental setup used for studying interaction of a drop with a flat plate is shown in Figure 1. The setup consists of a dropper for drop generation, a flat surface on which drop impact was studied, a high-speed CCD camera (from Redlake Imaging, San Diego, CA) for image capturing, flashlight, and image processing software Image Pro (from Media Cybernetics, Silver Spring, MD). Drops were generated manually with a dropper. Droppers with inner diameter of 4 and 0.5 mm and liquids with different surface tension and contact angle (distilled water with or without SDS and mercury) were used to generate drops of diameters ranging from 2.5 to 4.2 mm. Surface tension of water was reduced with the help of SDS (0.094 g SDS was added in 20 mL of water). This concentration of SDS is well beyond the critical micellar concentration (8.2 mM). Two solid surfaces, glass and Teflon, were chosen for the study such that it is possible to cover the relevant range of contact angle (CA).

It was observed that the water drop on a glass surface shows varying CA during the process of drop spreading and recoiling. This is attributed to adsorption of moisture on the glass surface. To minimize the effect of surface moisture on contact angle, the surface was washed with hot water, dried at 80°C for 0.5 h, and then cooled in a dry environment before performing the experiments. Experiments were carried out on a pretreated (dry) glass surface as well as on a non-pretreated surface. The observed dynamics of drop impact with and without such treatment of glass surface showed significant differences (discussed below). A Teflon surface was created with the help of Teflon tape wrapping on an acrylic surface. From experiments it was observed that the drop contact angle remains constant for a prolonged time once it achieves equilibrium, which indicates that there is negligible effect of adsorbed moisture on drop dynamics, and thus no surface pretreatment was needed during the experiments.

A liquid drop formed at the tip of the dropper was allowed to fall freely onto the solid surface placed below the dropper. The desired drop impact velocity was achieved by varying the dropper height from the plate surface. Drop impact velocity was measured just before the impact on the solid surface using image analysis software provided by Redlake Imaging. Recorded images were processed with the image analysis software, Image Pro plus (Media Cybernetics). Drop shape (diameter and height) was measured just before the impact. At high impact velocity (>1 m/s), some deviation from a spherical shape was observed. Experiments were repeated several times to ensure that the generated drop size is close to a predefined value and sphericity (d_{min}/d_p, where d_{min} is the minimum diameter of a compressed drop) is >0.98. Drop diameter just before the impact, drop impact behavior, and dynamics were recorded with the help of a high-speed CCD camera. Recording was carried out at various frame speeds, from 250 to 500 frames per second (fps). No significant information loss was observed between 125 to 500 fps for drop impact velocities up

to 1 m/s. Therefore, data for lower values of impact velocity (~0.2 m/s) were recorded at 250 fps, whereas for high values of impact velocity (~1 m/s), a recording speed of 500 fps was used. This high recording speed ensured that a minimum of eight data points were collected per period of oscillations and there was no loss of critical information between two consecutive frames. The camera was located at 15 cm from the dropper and a zoom lens (18–180/2.5) was used for recording the images. The camera was focused on an area of about 10 × 10 mm and images (of resolution > 75 dots/in.) were acquired in a movie form. A bright white light was used in front of the camera and a light diffuser was used in between so as to remove harsh shadows from the object.

Recorded images were processed with the image analysis software, Image Pro plus (Media Cybernetics). For calibration, a test material of known dimension was recorded during each set of experiments. Brightness and contrast of the images were adjusted so that a clear three-phase interface position could be measured. Variations of dynamic contact angle (DCA), drop height, and diameter with time were measured (see Figure 1b) with Image pro plus. Drop oscillations usually are damped in about 0.5 s. The images of stationary drop were acquired after ensuring that all the oscillations were damped out (~3 s). Values of measured static contact angle (SCA) of water on glass and Teflon surfaces were found between 35–75 and 110–125°, respectively. Unlike the glass surface, the measured values of SCA for the Teflon surface were rather insensitive to moisture and other surrounding conditions. Measured drop height and diameter were made dimensionless by dividing them by the values of drop height and diameter measured when the drop comes to complete rest. The variations in DCA and dimensionless height or diameter were plotted against time (made dimensionless using measured value of average oscillation time). Drop impact experiments were performed for several times to ensure that the measured profiles of drop height/diameter with respect to time are within ±5%.

Computational Model

Several methods are available to simulate free surface flows (see, for example, Fukai et al., 1995; McHyman, 1984; Monaghan, 1994; Ranade, 2002; Unverdi and Tryggvason, 1992). Free-surface methodologies can be classified into surface tracking, moving mesh, and fixed mesh (volume tracking) methods. Surface tracking methods define a sharp interface whose motion is followed using either a height function or marker particles. In moving mesh methods, a set of nodal points of the computational mesh is associated with the interface. The computational grid nodes are moved by interface-fitted mesh method or by following the fluid. Both of these methods retain the sharper interface. However, mesh or marker particles have to be relocated and remeshed when the interface undergoes large deformations. As the free surface deformation becomes complex, the application of these methods becomes very computationally intensive. Another method, which can retain a sharp interface, is the boundary integral method (Davidson, 2002). However, use of this method is still mainly restricted to two-dimensional (2-D) simulations.

The volume of fluid (VOF) method, developed by Hirt and Nichols (1981), is one of the most widely used methods in modeling of free surfaces. This is a fixed-mesh method, in which the interface between immiscible fluids is modeled as the discontinuity in characteristic function (such as volume fraction). Several methods are available for interface reconstruction such as SLIC (simple line interface calculation), PLIC (piecewise linear interface calculations), and Young's PLIC method with varying degree of interface smearing (see, for example, Ranade, 2002; Rider and Kothe, 1995; Rudman, 1997 for more details). In the present work, the VOF method (with PLIC) was used to simulate drop impact on the solid surfaces. Gas and liquid phases were modeled as incompressible, Newtonian fluids with constant value of viscosity and surface tension. Flow was assumed to be laminar. It is important to model surface forces and surface adhesion (details are discussed in the Appendix) correctly. The continuum surface force (CFS) model, developed by Brackbill et al. (1992), was used in this work. Details of model equations are discussed below.

Model equations

The mass and momentum conservation equations for each phase are given by

$$\nabla \cdot \mathbf{V} = 0 \tag{1}$$

$$\frac{\partial \mathbf{V}}{\partial t} + \nabla \cdot (\mathbf{V}\mathbf{V}) = -\frac{1}{\rho}[\nabla P - \mu \nabla^2 \mathbf{V}] + g + \frac{1}{\rho}\mathbf{F}_{SF} \tag{2}$$

where $\mathbf{V}$ is the velocity vector, P is the pressure, and $\mathbf{F}_{SF}$ is the continuum surface force vector. This single set of flow equations was used throughout the domain and mixture properties as defined below were used. The density of the mixture was calculated as

$$\rho = \sum \alpha_k \rho_k \tag{3}$$

where a_k is the volume fraction of the kth fluid. Any other mixture property, ϕ, was calculated as

$$\phi = \frac{\sum \alpha_k \rho_k \phi_k}{\sum \alpha_k \rho_k} \tag{4}$$

When in a particular computational cell:

- $a_k = 0$: the cell is empty (of the kth fluid)
- $a_k = 1$: the cell is full (of the kth fluid)
- $0 < a_k < 1$: the cell contains the interface between the kth fluid and one or more other fluids

The interface between the two phases was tracked by solution of a continuity equation for volume fraction function as

$$\frac{\partial \alpha_k}{\partial t} + \mathbf{V}_k \cdot \nabla \alpha_k = 0 \tag{5}$$

The volume fraction for the primary phase (gas) was not solved and was obtained from the following equation:

$$\sum_k \alpha_k = 1 \tag{6}$$

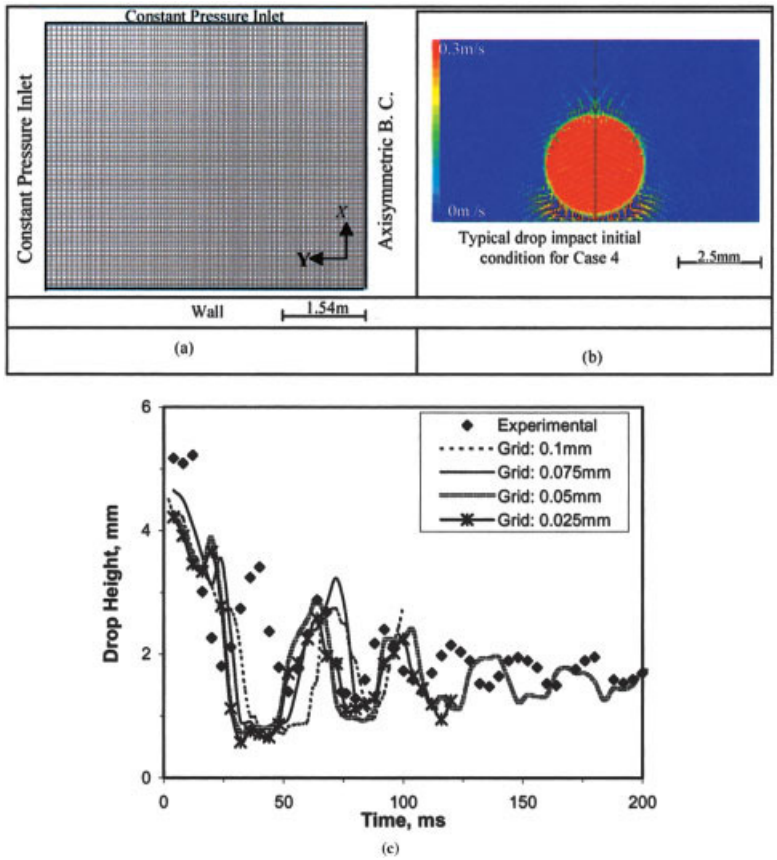

Figure 2. (a) Solution domain and boundary conditions. (b) Typical initial condition at $t = 0$. (c) Effect of grid size on oscillation of 4.2 mm drop on glass surface.

Average oscillation period = 26; equilibrium drop height = 1.55 mm.

In addition to the mass and momentum balance equations, surface tension and wall adhesion must be accounted for. Surface tension was modeled as a smooth variation of capillary pressure across the interface. Although representing the surface force in the form of volumetric source terms, stresses arriving as a result of a gradient in the surface tension were neglected. Following Brackbill et al. (1992), it was represented as a continuum surface force ($\mathbf{F}_{SF}$) and was specified as a source term in the momentum equation as

$$\mathbf{F}_{SF} = \sigma\kappa\mathbf{n}\left[\frac{\alpha_1\rho_1 + \alpha_2\rho_2}{1/2(\rho_1 + \rho_2)}\right] \tag{7}$$

$$\mathbf{n} = \nabla\alpha_2 \tag{8}$$

$$\kappa = -(\nabla\cdot\hat{\mathbf{n}}) = \frac{1}{|\mathbf{n}|}\left[\left(\frac{\mathbf{n}}{|\mathbf{n}|}\cdot\nabla\right)|\mathbf{n}| - (\nabla\cdot\mathbf{n})\right] \tag{9}$$

where $\mathbf{n}$ is the surface normal, $\hat{\mathbf{n}}$ is the unit normal, and κ is curvature. Surface normal $\mathbf{n}$ was evaluated in interface-containing cells and requires knowledge of the amount of volume of fluid present in the cell. A geometric reconstruction scheme (based on piecewise linear interface calculation, or PLIC) was used to calculate the interface position in the cell. Details of geometric reconstruction scheme are discussed in the Appendix. Adhesion to the wall influences the calculation of surface normal. Formulation and implementation of boundary conditions are discussed after describing the solution domain and the computational grids.

Solution domain and computational grid

From experimental images it was observed that drop spreading is symmetric at low liquid velocities (<1 m/s). Therefore, for low-impact velocities (<1 m/s), an axisymmetric 2-D domain was used to carry out simulations of drop impact. For impact velocities > 1 m/s, a 3-D domain was considered and the need of a 3-D domain for this case is discussed later in the Results and Discussion section. To minimize demands on computational resources without jeopardizing the ability to capture key features, the solution domain for such 3-D simulations was restricted to 90° with two planes of symmetry (instead of the full 360°). The axis-symmetric solution domain is shown in Figure 2.

The computational grid was generated using GAMBIT 2.0 (Fluent Inc., Lebanon, NH). Because the free surface between gas and liquid significantly changes shape and location during the course of VOF simulations, a uniform grid (with aspect ratio of unity) near the vicinity of the drop ($1.5 \times d_p$) was used and beyond that a nonuniform grid was used to reduce computational demands. Experimental information was used to

select the appropriate solution domain (such that they were at least 1.5 to 2 times maximum spreading and maximum height achieved during oscillations). During simulations, the flow field near the outer surfaces was monitored to ensure that no significant flow occurs there, which indirectly indicates that the size of the domain would not affect the simulation results. Simulations were initially carried out using different grids (see Figure 2c). These results are discussed later in the Results and Discussion section.

Boundary conditions and numerical solution

Boundary conditions used in the present work are shown in Figure 2a. Along the symmetry axis (x-axis in Figure 2a), a symmetric boundary condition was imposed in which normal velocity and normal gradients were set to zero, that is

$$u = 0 \qquad \frac{\partial v}{\partial x} = 0 \tag{10}$$

A no-slip boundary condition was used at the wall where all the components of velocity were set to zero. Treatment of wall adhesion and movement of the gas–liquid–solid contact line deserves special attention. When a liquid drop spreads on a solid surface (see Figure A2), wall adhesion modifies the surface normal as

$$\hat{\mathbf{n}} = \hat{\mathbf{n}}_w \cos\,\theta_w + \hat{\mathbf{t}}_w \sin\,\theta_w \tag{11}$$

where $\hat{\mathbf{n}}_w$ and $\hat{\mathbf{t}}_w$ are the unit vector normal and tangential to the wall, respectively, and θ_w is the contact angle at the wall. When the contact angle is zero, complete wetting occurs and the drop spreads on solid surface without oscillations. Although the no-slip boundary condition (zero velocity on wall) was implemented at the wall boundary, the gas–liquid–solid contact line moves along the wall, presenting a kind of singularity. Details of implementation of the wall adhesion boundary condition and how the singularity was bypassed in the numerical solution are discussed in the Appendix. Because velocity profiles at the other two planes (other than symmetry and wall planes) of the solution domain are not known, a constant pressure boundary condition was used at these planes.

The system of model equations was solved with the boundary conditions discussed earlier using the commercial flow solver Fluent 6.0 (Fluent Inc.). Mass and momentum equations were solved using a second-order implicit method for space and a first-order implicit method for time discretization. Pressure interpolation was performed using a body force–weighted scheme. This scheme is useful when the body force is comparable to pressure force. Body force–weighted pressure interpolation assumes continuity of ratio of gradient of pressure and density. This ensures that any density-weighted body force (such as gravity force) is balanced by pressure. This scheme performs better for VOF simulations of cases with fluids having a substantial density difference. Pressure implicit with splitting of operator (PISO) was used for pressure velocity coupling in the momentum equation. This scheme was used to reduce the internal iteration per time step and (relatively) larger underrelaxation parameters can be used.

The initial position of the liquid drop was obtained from recorded experimental data and sphere (assuming the drop was spherical) at the corresponding position was marked in the computational domain. The liquid-phase volume fraction was patched as unity ($\alpha_2 = 1$) in this marked sphere. Drop impact velocity was measured from images acquired by the CCD camera and was assigned to the liquid phase while initiating the simulation. This condition was assumed to be the initial condition occurring at time $t = 0$ s. A typical developed flow field inside and around the drop after five to six internal iterations is shown in Figure 2b (assumed as $t = 0$ s). A time step between 1 and 5 μs was found to adequately capture key features of drop impact dynamics (simulations using 2×10^{-6} and 4×10^{-6} showed no significant difference in the predicted results). Twenty to 30 internal iterations per time step were performed, which were found to be adequate for decreasing the normalized residuals to $<1 \times 10^{-5}$. With a further increase in time step (5×10^{-6}), required numbers of internal iterations were found to increase. Simulated results were stored for every 1- or 2.5-ms interval (adequate to capture key features of dynamics with timescales of about 16–25 ms). The liquid drop in the simulated results was identified from the computed isosurface of liquid volume fraction of 1.

Results and Discussion

Impact of drop on solid surface: physical picture/regimes

Behavior of a liquid drop after impact on a solid surface is determined by interactions of inertial, viscous, and surface forces. Drop diameter, impact velocity, liquid properties, and the nature of solid surface (such as CA, roughness, and contamination) are some of the key parameters. When a liquid drop makes an impact on a solid surface, it starts spreading on the surface. The kinetic energy of the drop is dissipated in overcoming viscous forces and in creating new surface area. Surface tension, acting at interfaces, resists spreading of the drop and eventually initiates recoiling. The kinetic energy of a drop increases during the recoiling process. Because of inertial flow, the drop height increases until all the kinetic energy is converted into potential energy. If the inertia developed during the recoiling is large enough to lift the drop away from a solid surface, the drop rebounds; otherwise, it starts spreading once again after achieving the maximum height. Such cycles of spreading and recoiling continue for quite some time. Depending on the surface tension and CA, drop oscillation behavior may exhibit different regimes. The fallen drop may spread on the solid (Figures 3a and b) or may just show a bulging at the center (Figure 3c). If the surface is contaminated (here adsorbed moisture) drop spreading is larger (Figure 3a), whereas if the surface is pretreated well (drying) the drop height is much larger (Figure 3b). The drops, which spread on the solid surface as shown in Figures 3a–c, may recoil and oscillate. If there is sufficient energy while recoiling, drops may rebound (see Figure 3d) from the surface after recoiling (see, for example, Mao et al., 1995; Richard and Quéré, 2000). Surface wetting (CA) plays an important role during this process. If the drop experiences less resistance at the surface (high CA) during recoiling, the drop may continue to rebound several times (like a bouncing liquid ball). In some cases, splashing may occur, resulting into several smaller droplets on the surface (Figure 3e).

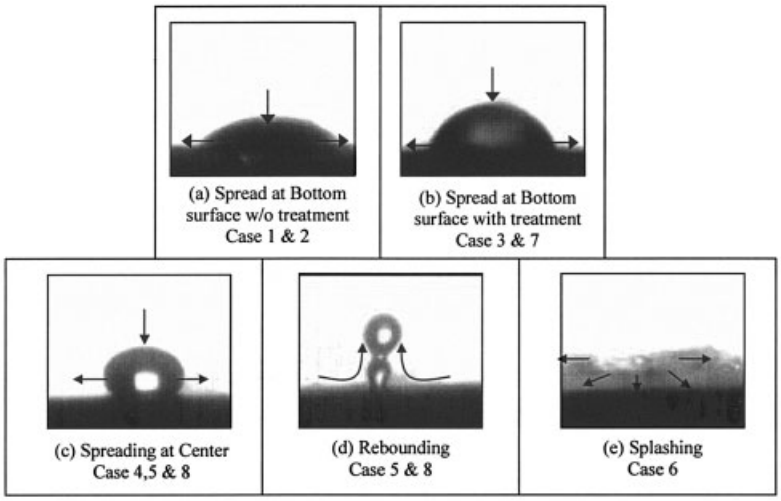

Figure 3. Drop spreading: spreading on glass (a and b) and on Teflon surface (c, d, and e).

In the absence of splashing, a liquid drop usually takes between 50 and 500 ms to come to rest. The final shape of the drop depends on the properties of the liquid and the solid surface. Even after coming to the so-called rest position, the drop continues to spread because of molecular movement at the surface to form a thin film, depending on the hydrophobic and hydrophilic nature of the surface. This phenomenon was not considered in this work. The scope was restricted to study key dynamic characteristics of the drop impact. To study key aspects of the different regimes of drop impact several parameters such as drop diameter, liquid properties (surface tension, viscosity, density), and surfaces were varied to cover the entire range of interest. Details of experiments carried out are listed in Table 2 along with the observed flow regimes.

Our experimental data and some of the published data are shown in Figure 4 in terms of Reynolds number (based on drop impact velocity) and modified Weber number (We_α). Although the data are not sufficient to clearly identify regime boundaries, it may be seen that the region in which the drop bounces from the surface increases as the value of We_α increases. Regimes observed in the simulated results are also shown in this figure. It can be observed that the CFD model was able to correctly capture the regimes. Results of the VOF simulations and sensitivity of the simulated results to different parameters are discussed in the following sections.

VOF simulations of a drop impact on the solid surface

Simulations for a 4.2-mm drop diameter with impact velocity 0.22 m/s (Re = 924, Ca = 332) were carried out in a 6 × 7-mm axis-symmetric domain. Simulations were first carried out with an average contact angle of 50° (We_α = 1.57) with different numbers of grids in the domain; 10, 13.3, 20, and 40 per mm. Drop height variation with time was compared with the experimental data in Figure 2c. It can be seen that simulated results with 20 mm and 40 grids per mm grids are not significantly different. Therefore, all the subsequent simulations were carried out with 20 grids per mm. As mentioned earlier, reduction in the time step below 4×10^{-6} s did not significantly affect simulated results and therefore all the subsequent simulations were carried out by setting the time step as 4×10^{-6} s.

To study the effect of the contact angle on simulated results, simulations were carried out at two values of contact angles (40 and 55°). The simulated variations in the drop height were plotted against time (see Figure 5). It can be seen that simulations with a contact angle of 55° are closer to the experimental values than those obtained with a contact angle of 40°. Values of the contact angle measured from the experimental images indicate that the value of the contact angle is initially higher (~55–60°), which subsequentlydecreases with time to about

Table 2. Operating Conditions and Dimensionless Numbers for Different Cases

			Properties										
Case	Liquid–Solid	V (m/s)	ρ_L (kg/m^3)	μ (Pa · s)	D_p (mm)	σ (N/m)	θ_w (°)	Re	We	Ca	We_α	Bo	Regime
1	Water–Glass	0.22	1000	1e-3	4.2	0.073	40	924	2.78	332	1.57	2.4	Oscillation
2	Water–Glass	0.3	1000	1e-3	2.5	0.073	35	750	3.12	240	1.69	0.85	Oscillation
3	Water–Glass	0.3	1000	1e-3	2.5	0.073	64	750	3.12	240	2.14	0.85	Oscillation
4	Water–Teflon	0.3	1000	1e-3	2.5	0.073	110	750	3.12	240	4.68	0.85	Rebound
5	Water–Teflon	1	1000	1e-3	2.5	0.073	110	2555	35.2	72	52	0.85	Rebound
6	Water–Teflon	4	1000	1e-3	2.5	0.073	110	10,200	566.6	18	832	0.85	Splash
7	Water + SDS–Teflon	0.3	1000	1e-3	2.5	0.038	75	750	5.92	127	4.11	1.61	Oscillation
8	Mercury–Teflon	0.45	13500	1.5e-3	2.75	0.46	180	10,300	15.15	681	<10,000	1.79	Rebound

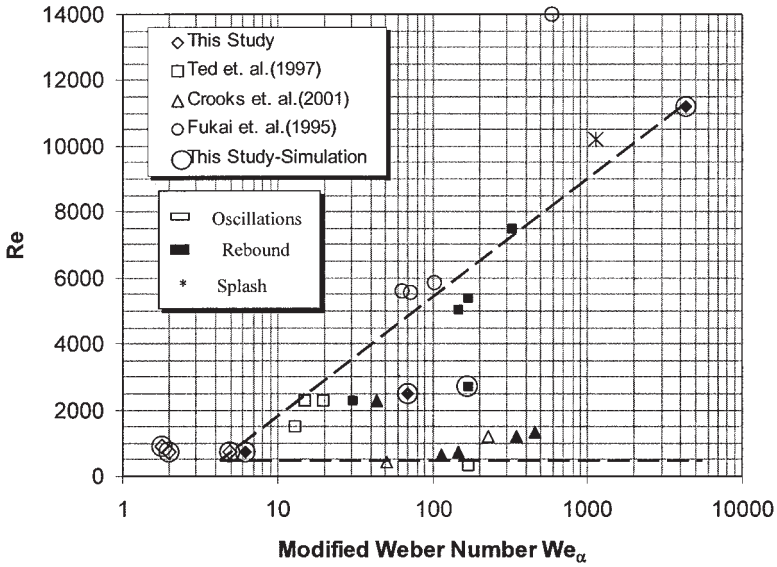

Figure 4. Drop impact on solid surfaces: oscillations of spreading and recoiling with or without rebound.

40° (see Figure 5). It can be seen that the measured values of the contact angle exhibit maximum or minimum corresponding to spreading or recoiling stage, respectively. In other words, the advancing contact angle is always higher than the receding contact angle. Values of the advancing and receding contact angles were found to decrease with each subsequent oscillation (see Figure 5). Considering the significant variation in the measured contact angle, CFD simulations were carried out with time-varying values of contact angle. Instead of including all the observed oscillations in the measured contact angle, numerical simulations were carried out with averaged values of contact angle [stepwise time variation of the contact angle was used (typically 15 steps) to represent the observed variation during the drop impact process]. Simulated results of the drop height variation (normalized with equilibrium drop height) with time, using such varying values of the contact angle, are also shown in Figure 5. It can be seen that agreement is better than that observed with the two previously discussed cases (that is, using contact angles of 40 and 55°). Thus all further simulations for a glass surface were carried out using stepwise time variation of averaged contact angle.

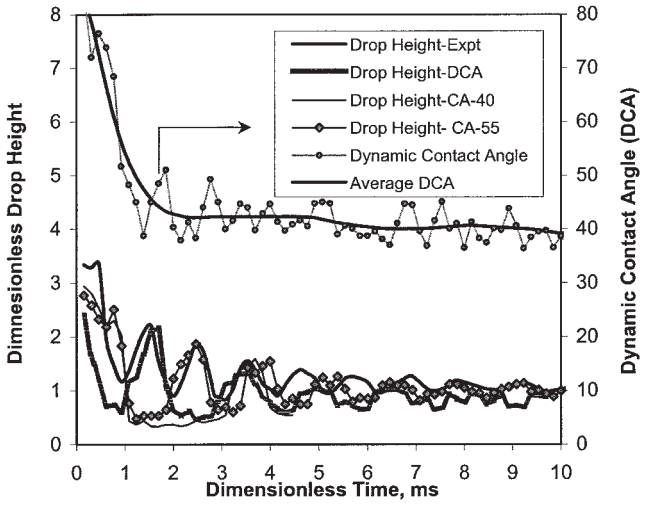

Figure 5. Comparison of simulated results with the experimental data for 4.2-mm drop.

Case 1: average oscillation period = 26; equilibrium drop height = 1.55 mm.

Simulated results of the drop impact process using dynamic contact angle were compared with the experimental images in Figure 6. After the impact on solid surface, the drop starts to deform and spread (Figures 6b–6e). As the drop spreads, the drop height and spreading velocity decreases, which causes decreases in kinetic and potential energy of the drop. After maximum spread, surface forces acting on the drop try to reduce the surface area of the drop by reversing the spread (recoiling). At this point, the drop height starts to rise from the center (see Figures 6f–6h). Developed inertia during the recoiling process lifts the drop height to a considerable extent. Beyond a certain increase of drop height (Figures 6g and 6h)—once the kinetic energy is converted into the potential energy—the drop starts to fall (Figure 6i) under the influence of gravity. This process continues until the drop comes to the equilibrium position. It can be seen that the simulations were able to capture the key features of spreading and recoiling. The quantitative agreement between experimental and simulated results was improved by implementing time variation of the contact angle. The computational model was further evaluated by carrying out simulations for different system parameters. Both experimental and computational results, required to understand the effects of various parameters on the dynamical behavior of a drop, are discussed in the following sections. Possible reasons for the observed deviation of simulated results from experimental values are discussed after that.

Influence of the system parameters on dynamics of drop impact

Influence of Drop Diameter. The influence of the drop diameter on the dynamics of spreading and recoiling of the drop was studied by carrying out experiments with falling

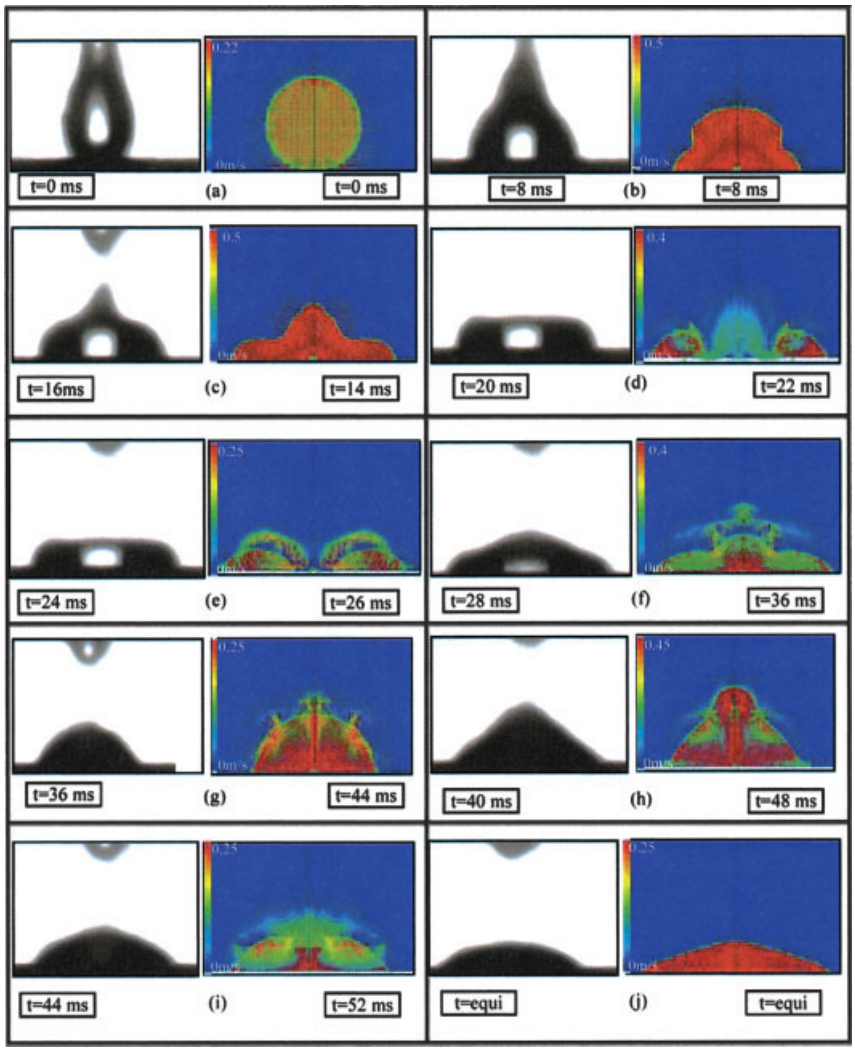

Figure 6. Comparison of the experimental and simulation results of the drop dynamics for 4.2-mm drop.

Case 1: impact velocity = 0.22 m/s; drop diameter = 4.2 mm; solid surface: glass.

drops of diameters 2.5 and 4.2 mm (of water) onto a flat glass surface. Experimental observations for the case of a 4.2-mm-diameter drop are discussed in the previous section. The Reynolds numbers (750 and 924) are negligibly different for the cases of 2.5- and 4.2-mm drops. Experiments with a 2.5-mm drop showed oscillations that were substantially similar to those observed with the 4.2-mm drop. The Bond number $Bo = \rho g d_p^2/\sigma$, which reflects the relative importance of the gravitation and capillary effects, indicates that the capillary term is quite significant for the case of a 2.5-mm drop ($Bo = 0.85$) compared to that for a 4.2-mm drop ($Bo = 2.4$). Experiments with a 2.5-mm drop were carried out with both pretreated and non-pretreated glass surface. A non-pretreated glass surface contains moisture on the solid surface because of long exposure to the environment (25°C, atmospheric pressure and 76% humidity, nontreated surface). The observed variation of contact angle during the process of spreading and recoiling on a non-pretreated surface was considerably lower (max = 42°, min = 37°; see Figure 7a) than that observed on the pretreated surface (max = 90°, min = 65°; see Figure 7b). It appears that the presence of moisture on the nontreated glass surface considerably affects the drop dynamics.

The qualitative behavior of the smaller drop (of 2.5 mm diameter) was similar to that of 4.2 mm drop, including ring formation and cycles of spreading and recoiling. It can be seen that values of the time required for the drop to come to rest was reduced from 270 to 158 ms for a 2.5-mm drop and the average oscillation period for the 2.5-mm drop was almost 30% of that observed for the 4.2 mm drop (18.55 and 26 ms). The average amplitude ratio for the 2.5-mm drop was also reduced from 1.15 to 1.06. The maximum spread radius and maximum height achieved during the first cycle were found to be 3.4 and 1.7 mm, respectively. Impact simulations of a 2.5-mm drop on a flat glass surface were carried out at an impact velocity of 0.3 m/s. The average value of the dynamic contact angle variation with time was used for simulations. Simulated height variation with time was compared with the experimental results in Figure 7b. The maximum height achieved during the first cycle of oscillation was 2.42 mm, which is in reasonable agreement with the value obtained from simulations (2.62 mm).

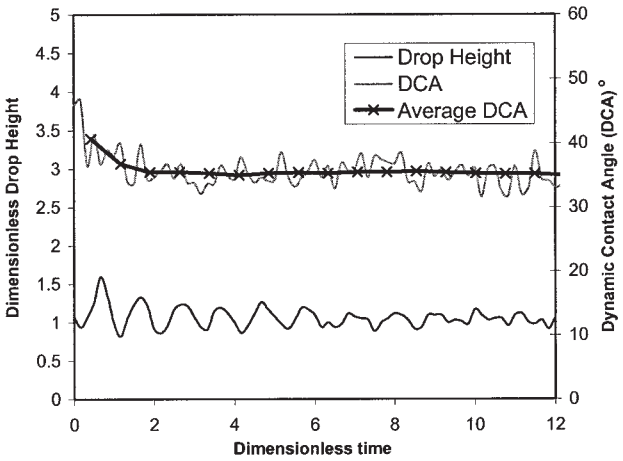

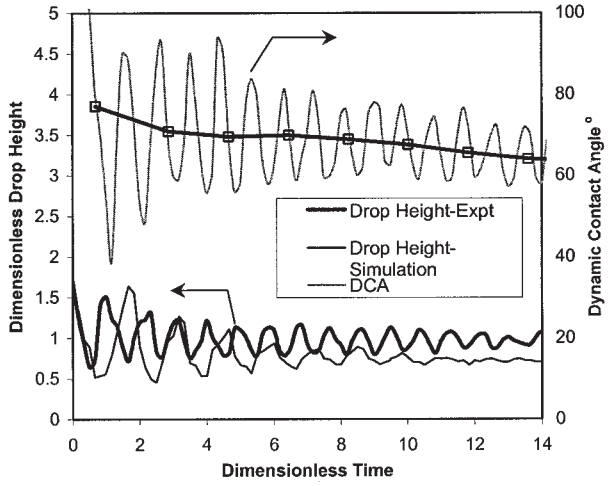

Figure 7. (a) Dynamics of drop height and contact angle for non-pretreated glass surface; (b) drop oscillations with time: dynamics of drop height and contact angle for pretreated glass surface and simulation comparison.

(a) Case 2: average oscillation period = 12; equilibrium drop height = 0.94 mm; (b) Case 3: average oscillation period = 11.33; equilibrium drop height = 1.6 mm.

Influence of Impact Velocity. Experiments were carried out to study the influence of impact velocity on the dynamics of a drop falling onto a Teflon surface. A Teflon surface has less affinity to water molecules compared with a glass surface and thus the Teflon surface needed no pretreatment. A Teflon–water SCA was found in the range of 110–120°. A water drop falling onto a Teflon surface showed results that were significantly different from those of a drop falling onto a glass surface. The drop rebounded from the Teflon surface even at lower impact velocities (0.3–1 m/s). At high impact velocity (~4 m/s), the liquid drop was found to disintegrate and caused splashing (see Figure 3e). For this case, inertial forces dominate capillary forces (Re ~ 10,000, Bo = 0.85). At low liquid velocities, after rebound, the consecutive cycles showed spreading and recoiling behavior according to Figure 3c (that is, the bottom portion of the drop was not found to take part in spreading).

The experimentally measured variation of the drop height with time for the drop of diameter 2.5 mm and impact velocity of 0.3 m/s is shown in Figure 8. It can be seen that the drop height increases considerably during the first cycle of spreading and recoiling because of rebounding compared to the consecutive cycles. The oscillations arising from spreading and recoiling were continued even beyond 465 ms. Overall parameters such as average oscillation period and amplitude ratio were found to be 16.57 s and 1.03, respectively. The maximum spread diameter and maximum height achieved during the first cycle were found to be 3.9 and 3.25 mm, respectively.

Simulations, carried out with 2-D solution domains (5 × 6 mm), were found to capture the drop rebounding as well as the oscillation phenomenon. Comparison with experimental snaps of drop rebound during the first cycle is shown in Figure 9. Flow fields that developed around the drop after 2 ms are shown in Figure 9a. Simulated results captured trends that were similar to those observed in experiments. Simulations correctly showed drop spreading, recoiling, and rebounding (Figures 9c–g). During recoiling, the drop may trap a gas bubble, which is observed in simulated results (Figure 9d). Mehdi-Nejad et al. (2002) reported similar bubble entrapment inside an impacting drop. Complete lift of a drop (rebound) was observed during the recoiling process. Both the simulated and the experimental results indicate that the drop shows a secondary oscillation while entirely suspended in the air (see first cycle in Figure 8). When a drop rebounds to its maximum extent, the velocity of the top surface of the drop becomes zero and the top surface reverses the direction of movement under the influence of gravity. However, at this stage, the bottom region of the drop continues to move in an upward direction under the influence of inertia and surface forces. Such an upward movement of bottom surface interacts with the top surface and again forces the top surface to reverse its direction of movement. The top surface begins to move upward, exhibiting a secondary peak in a plot of drop height vs. time. Eventually both the bottom and

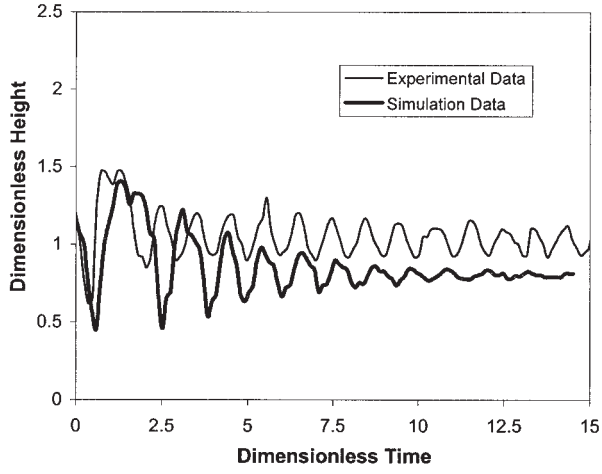

Figure 8. Comparison of the experimental data of drop height variation with simulated results.

Case 4: average oscillation period: 16.57 ms; final drop height: 2.2 mm.

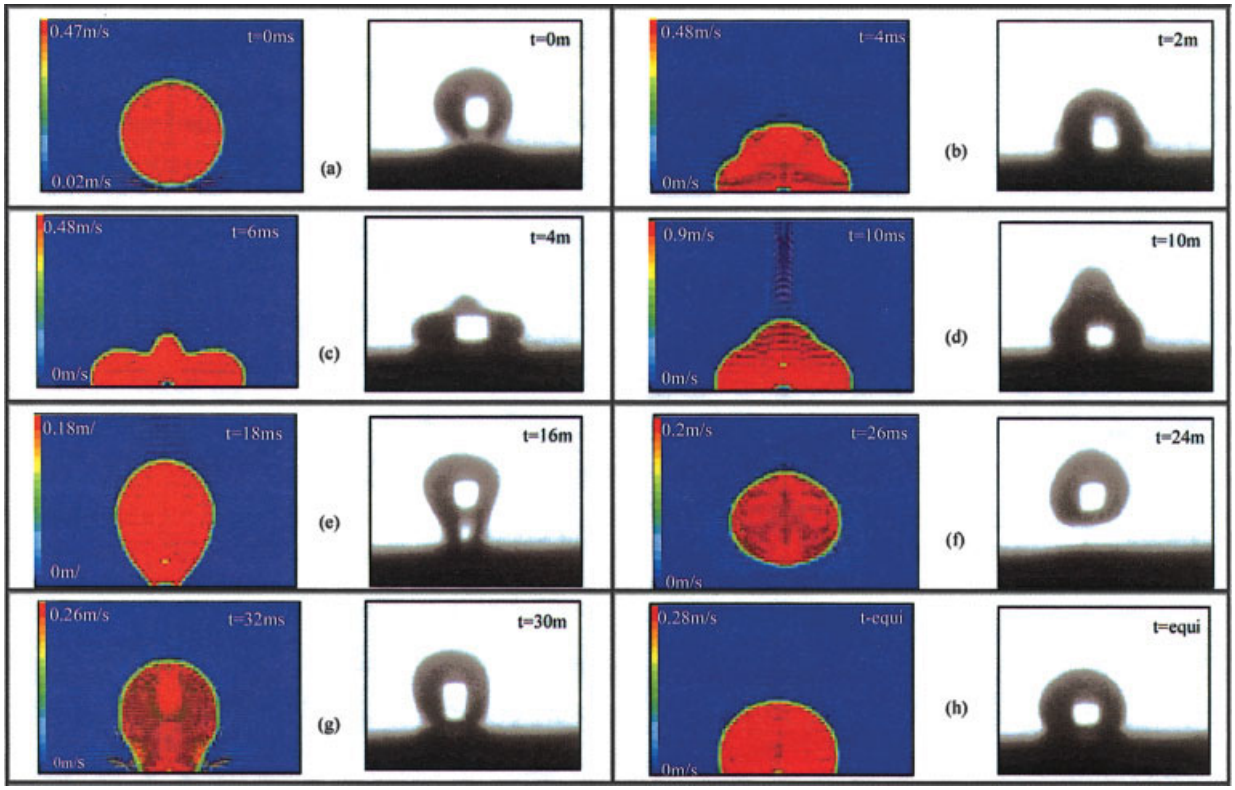

Figure 9. Contours and flow field of spreading and rebounding drop.

Case 3: average oscillation period: 16.57 ms; final drop height: 2.2 mm.

the top regions of the drop reverse the direction of movement under the influence of gravity and the drop starts falling down. It can be seen that simulations captured the rebound phenomena (including secondary oscillations) and subsequent oscillations of spreading–recoiling and can provide complete flow fields of gas and liquid phases. Use of such a flow field for better understanding of interphase closures is discussed in a later subsection.

To quantify these results, simulated drop height variation was compared with the experimental measured data (see Figure 8). It can be seen that the predicted oscillation time is greater than the experimentally observed value. Unlike the experimental observations, where the drop spreads from the middle (Figure 3c), simulated results indicate spreading at the bottom. The bottom spreading causes overprediction of oscillation time because of greater resistance offered by the solid surface. In simulation liquid–solid interaction is greater than that observed in experiments (almost negligible because the contact line moment is zero). To achieve this in simulation one needed to assign the zero moment of contact line on solid surface.

With higher drop impact velocity (Case 4: 1 m/s), overall behavior was similar to the case with lower impact velocity (Case 3), that is, spreading, recoiling, rebounding, and subsequent oscillations (according to Figure 3c). High-speed images acquired for this case indicated the average oscillation period as 24 ms and average amplitude ratio as 1.05. The maximum spread was found to be 5.88 mm and maximum height achieved during the first cycle was 5.66 mm, which is about 40% greater than that observed at an impact velocity of 0.3 m/s. In 2D axis-symmetric simulations, drop breakage occurs near the top instead of at the middle and this causes formation of a smaller drop (lighter) after the breakage. Because of the formation of a lighter drop in the simulations, the simulated maximum height at which this drop travels is higher (11 mm) than that observed in the experiments (6 mm). Experimental observation indicates that during spreading, satellite drop formation process just begins at this impact velocity, which is not symmetric. There are three possible reasons for deviation from axis-symmetric spreading: variations in the nature of the solid surface, development of an instability, or deviation of the liquid drop from a spherical shape at impact. In our simulations, we had assumed the drop to be spherical and variations in solid surface were not taken into consideration. However, intrinsic instability can cause asymmetric spreading if symmetry is not imposed artificially. In 2-D simulations, symmetry is artificially imposed and thus 2-D simulations can never capture intrinsic instability and can never predict asymmetric spreading. It is essential to carry out a 3-D simulation to capture such asymmetric drop spreading.

To reduce the computational demands, in this work we have considered only a 90° sector of the full 3-D domain (when viewed from the direction of a drop fall). Appropriate formulation of boundary conditions at the vertical planes bounding the 90° sector (and passing through symmetry axis) is needed. Three-dimensional simulations will be equivalent to 2-D simulations if rotational periodic boundary conditions are imposed on these planes. With these boundary conditions, results of 2-D and 3-D simulations will be identical. We had thus used symmetry boundary conditions on these planes in our 3D simulations. Unlike periodic boundary conditions, these boundary

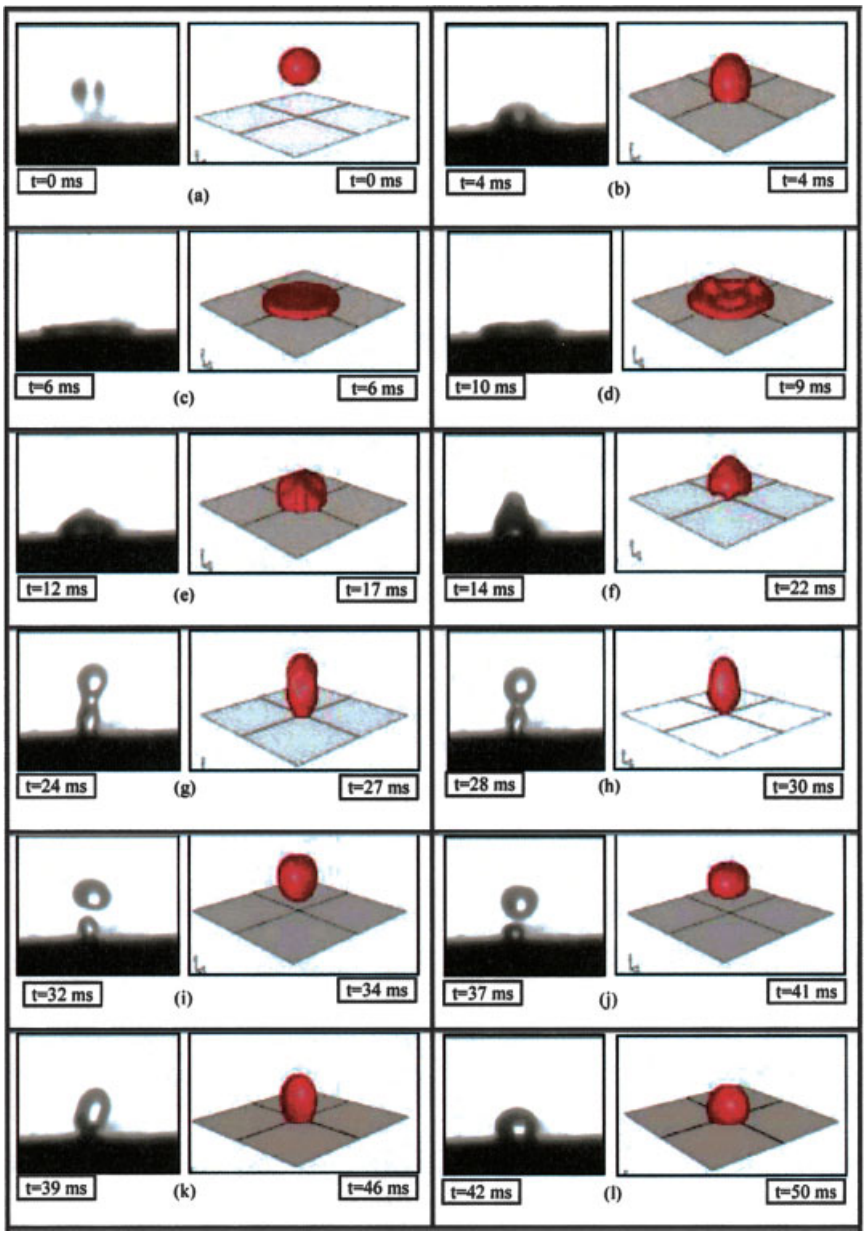

Figure 10. Comparison of the drop dynamics with simulation results of drop impact on Teflon surface.

Case 5: impact velocity: 1 m/s; drop diameter: 2.5 mm; solid surface: Teflon.

conditions do not tightly impose axis-symmetry, although locally symmetric conditions are enforced. For low values of impact velocity, where drop spreading is symmetric, we had obtained identical results from our 2-D and 3-D simulations.

At higher impact velocity (1 m/s and above), asymmetry in drop spreading was observed experimentally. To evaluate whether the computational model can capture asymmetric spreading, we had carried out 3-D simulations with symmetry boundary conditions. The size of the solution domain was 5 × 5 mm in width and length and 6 mm in height. Simulations were carried out using 0.1-mm grid size. Because of the excessive demands on computational resources, 3-D simulations could not be carried out beyond the first cycle of the oscillations. Despite this, the simulated behavior of the drop was found to be very similar to that observed in the experiments and was able to capture the key features reasonably well (Figures 10a–k). Rebound of the drop during recoiling (which was also observed by Mao et al., 1995; Richard and Quéré, 2000) was also captured reasonably well in the simulations (Figures 10g and h).

Influence of Contact Angle and Surface Tension. The influence of contact angle was studied by comparing drop dynamics of a 2.5-mm water drop at an impact velocity of 0.3 m/s onto a glass and a Teflon surface (Cases 3 and 4). The modified Weber number (We_α) increases significantly with increasing contact angle for the same Reynolds and Weber numbers. The experimentally measured variation of drop height with time is shown in Figure 11. It can be seen that the water drop comes to rest much earlier on a glass surface (126 ms) than on a Teflon Surface (>468 ms). The

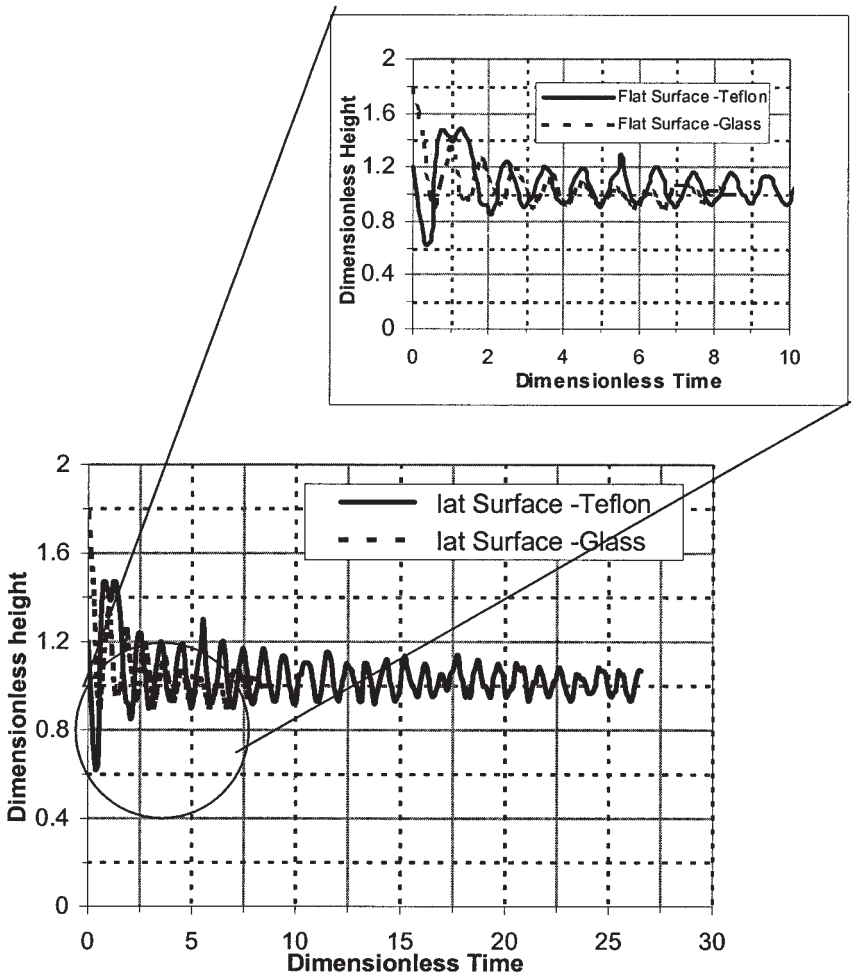

Figure 11. Comparison of drop dynamics on glass and Teflon surface.

Experimental conditions: Case 3; liquid: water; solid surface: Teflon and glass; impact velocity: 0.3 m/s.

water drop on a glass surface (CA = 55°) spreads at the bottom (see Figure 3a), where viscous dissipation at the solid–liquid interface damps spreading and recoiling oscillations. On a Teflon surface (CA = 120°), however, liquid–solid interaction is quite small because the drop deformation occurs at the center of the drop (see Figure 3c). This causes oscillations to persist for much longer time than on a glass surface. The values of maximum spread diameter on a glass and a Teflon surface, however, are not very different (glass: 4.76 mm; Teflon: 3.69 mm).

Experiments were carried out with falling drops of SDS solution in water (16 mM solution). The surface tension and SCA on a Teflon surface were found to be 0.038 N/m and 64°, respectively (compared to 0.072 N/m and 120° for water). With SDS solution, the time required for the drop to come to rest was much lower than that with water (180 ms compared to >468 ms for water). The average oscillation time was reduced to 12.6 ms for SDS solution from 17.6 ms for water. It was observed that with SDS solution (lower surface tension and lower SCA), the drop deformation occurs according to a bottom spreading mechanism, as shown in Figure 3b instead of 3c. Variation of dynamic contact angle is shown in Figure 12. For simulations, average values of the dynamic contact angle were used. Comparison of simulated drop height variation with time with experimental data is shown in Figure 12. Simulations show a sluggish response compared to the experimental data.

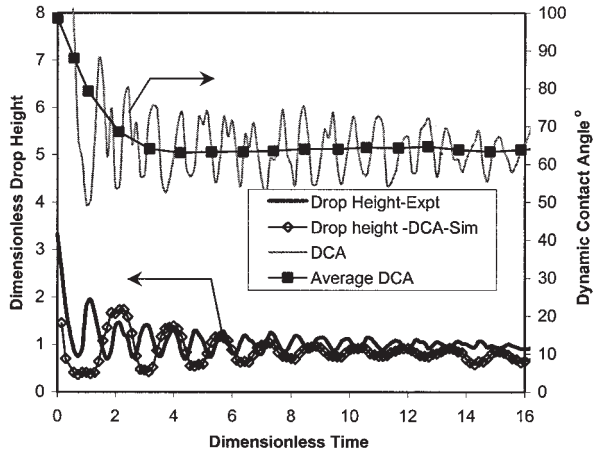

Figure 12. Comparison of the experimental data of drop height variation with simulated results.

Case 7: average oscillation period: 14 ms; final drop height: 1.5 mm.

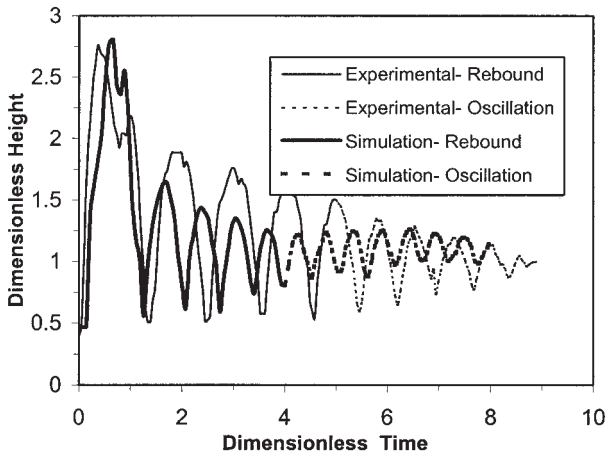

Figure 13. Comparison of the experimental and simulation results of the mercury drop dynamics.

Case 8: average cycle frequency: 54; final drop diameter: 2 mm.

Influence of Nonwetting Behavior on Drop Dynamics. Experiments were carried out with mercury drops to understand the influence of nonwetting behavior (static contact angle of nearly 180°). The mercury also has a very high density (13,000 kg/m^3) and surface tension (0.4 N/m) compared to those of water. Experiments were performed with mercury drops falling onto a Teflon surface at an impact velocity 0.45 m/s. Mercury drops rebounded several times before exhibiting the usual oscillations of spreading and recoiling. Spreading/recoiling behavior was similar to that exhibited by a water drop on a Teflon surface. Experimentally measured variation of drop height with time is shown in Figure 13. The bouncing region and oscillation region are indicated with continuous line and dotted line, respectively.

Simulations were carried out to simulate the impact of mercury drops on a Teflon surface. Comparison of simulated drop height variation with the experimental data is shown in Figure 13. Both experimental and simulated results show local minima during the first cycle. The average oscillation period was underpredicted in the simulated results (41.3 ms as compared to the experimental value, 54 ms). Simulated results were able to capture the multiple bouncing of a mercury drop as observed in the experiments.

Comments on Comparison of Experimental and Computational Results. It was shown that the VOF simulations captured the key characteristics such as drop spreading/recoiling, bouncing, and splashing reasonably well. It should be noted that because of inherent limitations in the VOF formulation, the interface is smeared across the grid size unlike the sharp interface in practice. Despite these limitations, the VOF simulations captured the drop interaction with solid surfaces reasonably well and provided detailed information about the flow field during such an interaction process. However, in general simulations overpredicted oscillation time and showed slower oscillations compared to those observed in the experiments.

It may be noted that VOF simulations, at present, are unable to account for microscopic surface characteristics such as roughness or contamination. It was observed from the experimental images that the contact angle exhibits continuous variation during the spreading and recoiling process. This variation is a strong function of surface characteristics and contamination. Because it was impossible to specify exact initial conditions (drop position and velocities) corresponding to the experiments in the VOF simulations, some differences in the experiments and simulations were not unexpected. A possible way to overcome these errors might be to include the drop formation process at the dropper while simulating. However, this would substantially increase the demands on computational resources. In the present work, therefore, some differences in the initial conditions between experiments and simulations were accepted under the constraints of available computing resources. The second possible source for the observed disagreement between experimental and simulated results is inadequate representation of varying contact angles in the simulations. As mentioned earlier, we used a stepwise approximation of the profile from a moving average of measured contact angles. If the initial conditions of experiments and simulations were identical, it might have been possible to specify the detailed variation of contact angle based on the measured values (without moving average and stepwise approximation). This may reduce the quantitative differences in the predictions and experimental data.

While making the quantitative comparisons between experimental and simulated results, it should be noted that any differences in initial conditions would amplify the differences between simulated and experimental results as time progresses. Any subsequent errors in specifying time-varying contact angle will further enhance the errors. Possible nonuniformities in surface roughness or adsorbed moisture may also lead to observed differences. Despite these possible sources of errors, it can be stated that the VOF simulations presented here were able to capture key processes in drop spreading, recoiling, and rebounding for a variety of systems. Because the CFD simulations can provide detailed information about flow field, these results can be used to gain better insight into drop interaction with a flat plate.

Interaction of Liquid Drop and Flat Surface. The flow field predicted by the VOF models can be used to examine various intricate details of interaction of a liquid drop and flat surface. Here we demonstrate this by using the simulated flow field to study energy balance and interphase interactions during spreading and recoiling.

During drop impact, spreading, and oscillation processes, kinetic, potential, and surface energies were interchanging between each other and loss of energy occurs through viscous dissipation. Simulated results were used to calculate kinetic energy, potential energy, and surface energy variation during the drop impact. Potential and kinetic energies of a drop were calculated by summing over all the computational cells. Surface energy (SE) was calculated as

$$\mathrm{SE} = A_{GL}\sigma_{GL} + A_{LS}(\sigma_{LS} - \sigma_{GS}) \tag{12}$$

where A_{GL} and A_{LS} are the interfacial area for gas–liquid and liquid–solid phases, respectively. σ_{LS}, σ_{GS}, and σ_{GL} are, respectively, the surface tension between liquid–solid interface, gas–solid interface, and gas–liquid interface. The unknown term σ_{GS} was eliminated by using the following Young–Dupre equation (Adamson, 1982):

$$\sigma_{GS} = \sigma_{LS} + \sigma_{GL}\cos\theta_w \tag{13}$$

where θ_w is the liquid–solid contact angle. Potential energy (PE), kinetic energy (KE), and surface energy (SE) were calculated by

$$\text{PE} = \sum_{1}^{n-cells} (h_{cell}\rho g)(Vol_{cell}) \tag{14}$$

$$\text{KE} = \sum_{1}^{n-cells} \left(\frac{1}{2}\rho V_{cell}^2\right)(Vol_{cell}) \tag{15}$$

$$\text{SE} = \sum_{1}^{n-cells} \sigma_{GL}[A_{GL} - (A_{LS}\cos\theta_w)] \tag{16}$$

The predicted variation of energies is shown in Figure 14 for glass and Teflon surfaces. When a drop spreads to its maximum extent and is about to recoil, its potential energy exhibits a minimum. Per cycle of potential energy, there are two cycles of kinetic energy because it passes through a maximum during spreading as well as recoiling. It can be seen that the amplitude of oscillations is higher for the glass surface than that for the Teflon surface. Scales of variation of surface energy are higher than the potential and kinetic energies and its variation is very sensitive to the variation in a contact angle. Therefore small errors in the values of contact angle or surface area may corrupt the calculation of total energy. To increase the robustness of the calculation of different components of energies, we have analyzed the variation of total viscous dissipation by using the following energy balance at time t

$$(\sigma_{SL}A_{SL})^0 + \text{PE}^0 + \text{KE}^0 + (\sigma_{GL}A_{GL})^0 = \text{KE} + \text{PE} + \sigma_{GL}A_{GL} + \sigma_{SL}A_{SL} + D \tag{17}$$

where the superscript 0 denotes quantities evaluated at the initial condition (at $t = 0$ s) and D is the total viscous dissipation until time t. The predicted variation of viscous dissipation with time is shown in Figure 15. Despite some fluctuations, the overall variation in dissipation curve shows an expected increasing trend.

The detailed flow field predicted by CFD simulations [typical sample of instantaneous flow field predicted by the VOF simulations is shown in Figure 16a (Case 3, at 7.5 ms after impact, 3D simulations for illustration)] can be used to compute other quantities of interest such as gas–liquid and liquid–solid interactions. Liquid–solid interaction can be determined by calculating the average shear stress exerted by the fluid on the solid surface. Gas–liquid interaction can be studied by calculating the strain rate on the gas–liquid interface. A detailed study of gas–liquid interaction (in terms of strain rate) and gas recirculation (in terms of vorticity) will be useful for various parametric studies such as interphase heat, mass, and momentum transfer for multiphase flows. Microscopic evaluation of these parameters would eventually be useful for developing better closure terms for complete reactor flow model.

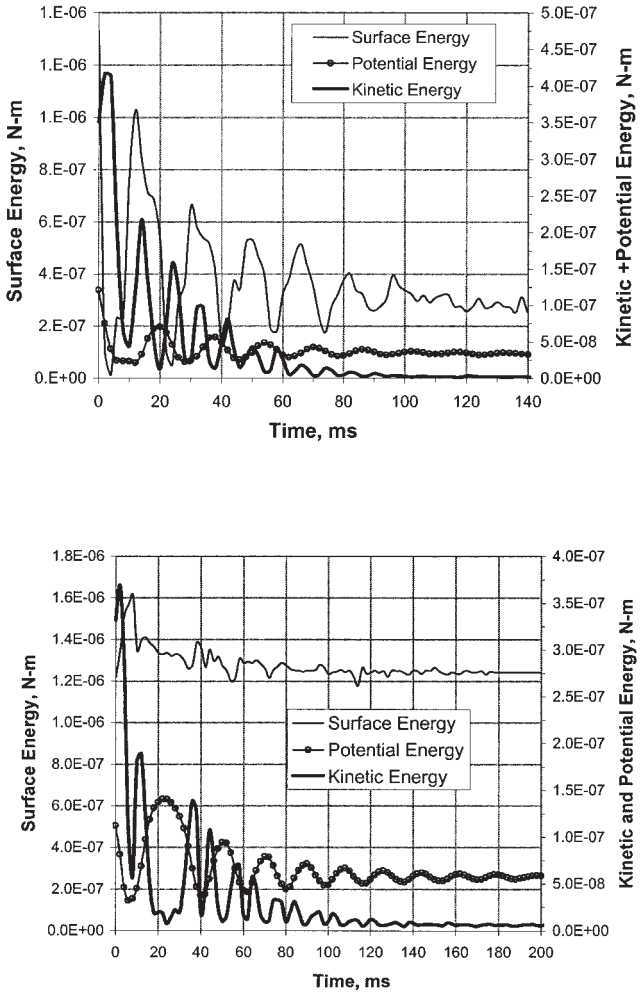

Figure 14. (a) Variation of the simulated surface, kinetic, and potential energy of drop during oscillations for Case 3; (b) variation of the simulated surface, kinetic, and potential energy of a drop during oscillations for Case 4.

Detailed calculations of these parameters for drop impact are discussed below.

The shear stress exerted by spreading liquid on solid surface was calculated as

$$\tau_w = \mu \frac{\partial V_i}{\partial x} \tag{18}$$

where V_i is liquid the velocity in the y-direction. Contours of the shear stress exerted on the wall are shown in Figure 16b. The maximum shear stress was observed in the region lying between the spreading edge and the central region. Gas recirculatory motion around the drop was quantified by calculating the vorticity as

$$\omega = \nabla \times V \tag{19}$$

The isosurface of the vorticity (a value of 2180 s^{-1}) is shown in Figure 16c. To define the shape of the drop, the isosurface of

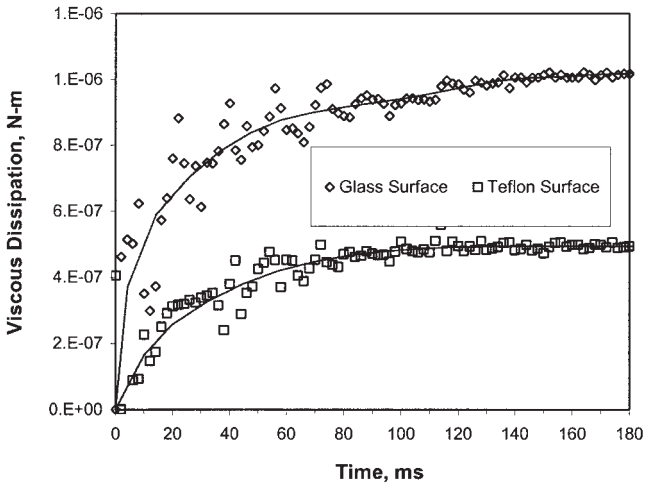

Figure 15. Variation of viscous dissipation with time for Cases 3 and 4.

the liquid-phase volume fraction of 1 is also shown in this figure (in red). It can be seen that high vorticity occurs at the spreading edge, intermediate ridge, and at the top surface of the drop. The contours of the strain rate on the isosurface of a liquid-phase volume fraction of 1 are shown in Figure 16d. Maximum strain rate was observed in the vicinity of high gas vorticity region.

The strain rate (area-weighted averaged) at the gas–liquid interface was calculated against time until the drop came to rest. The corresponding variation of the drop surface area (calculated from surface integral over the isosurface of liquid) along with the strain rate was plotted in Figure 17a. During each cycle of oscillation, the drop's velocity becomes zero during the end of the (1) spreading process and (2) recoiling process. The drop decelerates during the end of recoiling process and spreading process, and accelerates during the start of the spreading process and the recoiling process. During these periods the interaction between the phases is greater. It can be seen from Figure 17a that the strain rate is higher during the spreading process than during the recoiling process. A maximum drop interfacial area was observed when the drop spreads completely; strain rate is minimum at this point. The shear stress (area-weighted average) exerted by the flowing liquid over a solid surface was calculated during the drop oscillation. The shear stress and corresponding variation in the drop diameter are shown in Figure 17b. It can be seen that the shear stress on the solid surface increases during acceleration and deceleration processes. The shear stress during the spreading stage is always higher than that while recoiling.

Thus, VOF simulations of the type discussed in this work provide useful information about the interaction between gas and liquid as well as liquid and solid phases during the spreading and recoiling stages. These models have potential to account for solid surface curvatures (see, for example, Gunjal et al., 2005). Efforts are currently under way to extend these models to simulate spreading of liquid on curved surfaces of void space in a typical packed bed. Such efforts may eventually provide useful information about interphase interactions of gas–liquid flows in packed beds.

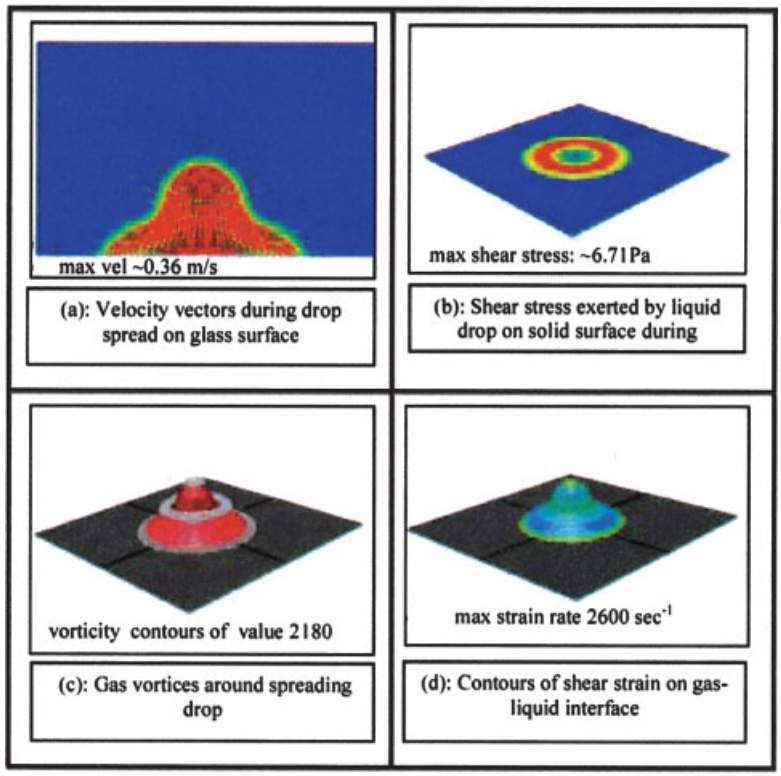

Figure 16. Illustration of gas–liquid and liquid–solid interaction during drop spreading on glass surface at time = 7.5 ms (Case 3).

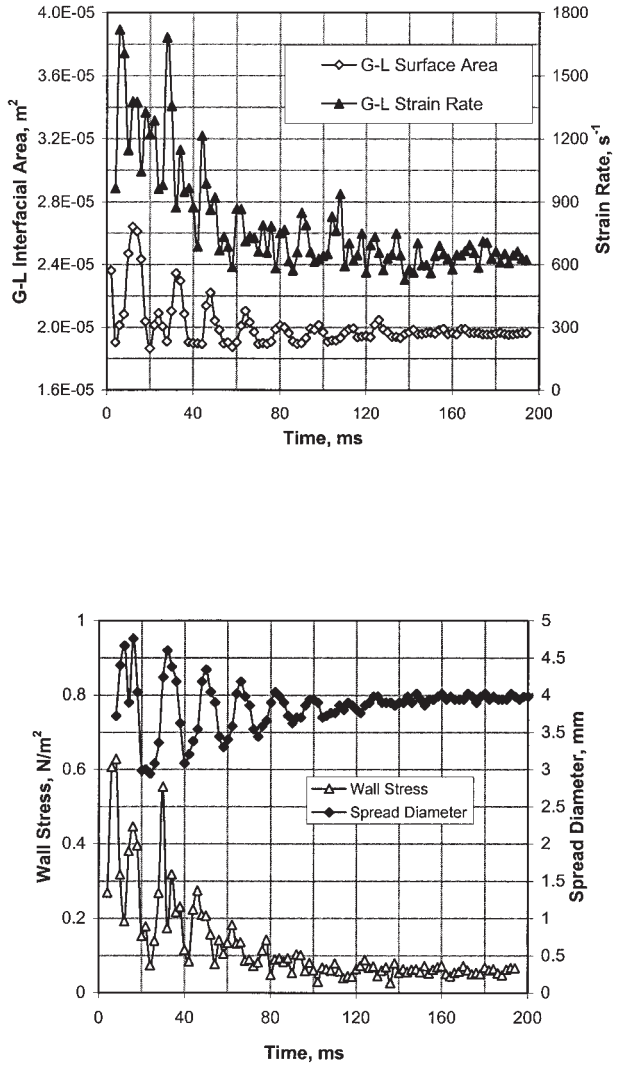

Figure 17. (a) Variation of average strain rate at gas–liquid interface and drop interfacial area during drop oscillations (Case 3). (b) Variation of average liquid–solid shear stress and drop diameter during drop oscillations (Case 3).

Conclusions

We have studied the dynamics of a drop impact process on a flat surface both experimentally and computationally. Experiments were carried out over a wide range of operating conditions (Re = 550–10,300; We_α = 1.5–10,000). Unlike most of the previous studies, the emphasis was on studying drop interaction with low-impact velocities (<1 m/s). Experimental data of drop deformation (shape/height/diameter) during spreading and recoiling (rebounding) processes were obtained until the drop attains an equilibrium position on a flat surface. Detailed VOF simulations were carried out and the predicted results were compared with the experimental data. These CFD simulations were also used to gain insight into drop interaction with flat surfaces. The key findings of the study are discussed below.

Dynamic variation of contact angle was found to be significant for liquid–solid systems whenever contact angles were low ($\theta_w <$ 90). Overall reduction of contact angle with time for water–glass or water–SDS–Teflon systems were much larger than that observed with water–Teflon or mercury–Teflon systems.

Adsorbed surface moisture (for glass surface) substantially alters the dynamics of the drop and dynamic variation of the contact angle was significantly larger for a pretreated glass surface than for a non-pretreated glass surface.

The average contact angle decreases during the oscillations of a drop. Agreement between simulated and experimental results was improved when average contact angle variation with time was used instead of using an equilibrium value.

The spreading mechanism affects the dynamics of drop and depends on the surface and liquid properties. For example, a 2.5-mm water drop on the Teflon surface was found to rebound (Case 4). When surfactant (SDS) was present, rebounding of water drops did not occur. VOF simulations also showed similar behavior.

Microscopic factors such as molecular movement of liquid contact line, surface roughness, and surface tension variation in the drop have the potential to considerably affect the drop dynamics. It is difficult to consider these processes in a model because of different spatial and temporal scales. Despite neglecting these processes, VOF simulations were found to capture reasonably well the key features of drop interaction (spreading/recoiling, rebounding, and breakup) with a solid surface.

In cases where the drop rebounded from a solid surface, the nose of a drop (uppermost point of drop) was found to exhibit local minimum while suspended in air. VOF simulations also showed similar behavior.

VOF simulations provide detailed information about the interaction between gas and liquid as well as liquid and solid phases. The models and approach presented here may be extended to understand spreading of liquid on curved surfaces of void space in a typical packed bed, which may eventually provide useful information about modeling of gas–liquid flows in packed beds.

Acknowledgments

One of the authors (P.R.G.) is grateful to Council of Scientific and Industrial Research (CSIR), India for providing Research Fellowship. The authors thank Professor Goverdhana Rao of the Indian Institute of Technology, Bombay for his constructive suggestions. The authors also acknowledge the anonymous reviewers who made numerous suggestions to improve the manuscript.

Notation

A_{GL}	gas–liquid interfacial area, m^2
A_{GS}	gas–solid interfacial area, m^2
A_{LS}	liquid–solid interfacial area, m^2
c	constant in Eq. A1
CA	contact angle, °
D	viscous dissipation, N·m
DCA	dynamic contact angle, °
d_{min}	minimum diameter of droplet during compression, m
d_p	droplet diameter, m
E_1, E_2	Ergun's constant
$\mathbf{F}_{SF}$	continuum surface force, kg m^{-2} s^{-2}
g	gravitational constant, m/s^2
h_{cell}	height of cell, m
L	length of bed, m
$\mathbf{n}$	surface normal vector
$\hat{\mathbf{n}}$	unit normal
$\hat{\mathbf{n}}_w$	unit normal at wall
P	pressure, Pa
SCA	static contact angle, °
SDS	sodium dodecyl sulfate

t time, s
$\hat{\mathbf{t}}_w$ unit tangent to the wall
V, v velocity, m/s
Vol_{cell} volume of cell, m^3

Greek letters

α volume fraction of phase
κ radius of curvature, m
μ viscosity, Pa·s
θ_w contact angle, °
ρ density of the fluid, kg/m^3
σ surface tension, N/m
σ_{GL} gas–liquid surface tension, N/m
σ_{LS} liquid–solid surface tension, N/m
σ_{GS} gas–solid surface tension, N/m
ω vorticity, s^{-1}

Dimensionless groups

Bo $\rho g d_p^2/\sigma$
Ca $\sigma/V\mu$
Re $\rho V d_p/\mu$
Oh $m/\sqrt{\rho\sigma d}$
We $\rho d_p V^2/\sigma$
We_α $\rho V^2 d_p/\sigma(1 + \cos\theta)$

Literature Cited

Adamson, A. W., *Physical Chemistry of Surfaces*, 4th Edition. Wiley, New York (1982).

Bergeron, V., D. Bonn, J. Y. Martin, and L. Vovelle, "Controlling Droplet Deposition with Polymer Additives," *Nature*, **405**, 772 (2000).

Brackbill, J. U., D. B. Kothe, and C. Zemach, "A Continuum Method for Modeling Surface Tension," *J. Comput. Phys.*, **100**, 335 (1992).

Bussmann, M., S. Chandra, and J. Mostaghimi, "Modeling of a Droplet Impacting on Solid Surface," *Phys. Fluids*, **12**, 3121 (2000).

Bussmann, M., J. Mostaghimi, and S. Chandra, "On a Three-Dimensional Volume Tracking Model of Droplet Impact," *Phys. Fluids*, **11**, 1406 (1999).

Chandra, S., and C. T. Avedisian, "On the Collision of a Droplet with a Solid Surface," *Proc. R. Soc. Lond. A*, **432**, 13 (1991).

Chandra, S., and C. T. Avedisian, "Observations of Droplet Impingement on a Ceramic Porous Surface," *Int. J. Heat Mass Transfer*, **35**, 2377 (1992).

Crooks, R., J. C. Whitez, and D. V. Boger, "The Role of Dynamics Surface Tension and Elasticity on the Dynamics of Drop Impact," *Chem. Eng. Sci.*, **56**, 5575 (2001).

Davidson, M. R., "Boundary Integral Prediction of the Spreading of an Inviscid Drop Impacting on a Solid Surface," *Chem. Eng. Sci.*, **55**, 1159 (2000).

Davidson, M. R., "Spreading of Inviscid Drop Impacting on Liquid Film," *Chem. Eng. Sci.*, **57**, 3639 (2002).

de Gennes, P. G., "Wetting: Statics and Dynamics," *Rev. Mod. Phys.*, **57**, 827 (1985).

Fukai, J., Y. Shiiba, T. Yamamoto, O. Miyatake, D. Poulikakos, C. M. Megaridis, and Z. Zhao, "Wetting Effects on the Spreading of a Liquid Droplet Colliding with a Flat Surface: Experiment and Modeling," *Phys. Fluids*, **7**, 236 (1995).

Fukai, J., Z. Zhao, D. Poulikakos, C. M. Megaridis, and O. Miyatake, "Modeling of the Deformation of a Liquid Droplet Impinging Upon at Surface," *Phys. Fluids A*, **5**, 2588 (1993).

Gladden, L. F., "Magnetic Resonance: Ongoing and Future Role in Chemical Engineering Research," *AIChE. J.*, **49**, 1 (2003).

Gunjal, P. R., V. V. Ranade, and R. V. Chaudhari, "Liquid Phase Residence Time Distribution in Trickle Bed Reactors: Experiments and CFD Simulations," *Can. J. Chem. Eng.*, **81**, 821 (2003).

Gunjal, P. R., V. V. Ranade, and R. V. Chaudhari, "Computational Study of Single-Phase Flow in Packed Bed of Spheres," *AIChE J*, accepted (2004).

Hirt, C. W., and B. D. Nichols, "Volume of Fluid (VOF) Method for the Dynamics of Free Boundaries," *J. Comput. Phys.*, **39**, 201 (1981).

Jiang, Y., M. R. Khadilkar, M. Al-Dahhan, and M. P. Dudukovic, "CFD of Multiphase Flow in Packed Bed Reactors: I. Modeling Issues," *AIChE J.*, **48**(4), 701 (2002).

Liu, D. Y., G. X. Wang, and J. D. Litster, "Unsaturated Liquid Percolation Flow through Nonwetted Packed Beds," *AIChE J.*, **48**(5), 953 (2002).

McHyman, J., "Numerical Methods for Tracking Interfaces," *Physica D*, **12**, 396 (1984).

Mehdi-Nejad, V., J. Mostaghimi, and S. Chandra, "Effect of Surrounding Gas on Droplet Impact," Proc. of 8th CFD Society of Canada, Montreal, Quebec, June 11–13, pp. 567–574 (2000).

Monaghan, J. J., "Simulating Free Surfaces with SPH," *J. Comput. Phys.*, **110**, 399 (1994).

Mourougou-Candoni, N., B. Prunet-Foch, F. Legay, M. Vignes-Adler, and K. Wong, "Influence of Dynamic Surface Tension on the Spreading of Surfactant Solution Droplets Impacting onto a Low-Surface-Energy Solid Substrate," *J. Colloid Interface Sci.*, **192**, 129 (1997).

Pasandideh-Fard, M., S. Chandra, and J. Mostaghimi, "A Three-Dimensional Model of Droplet Impact and Solidification," *Int. J. Heat and Mass Transfer*, **45**, 2229 (2002).

Pasandideh-Fard, M., Y. M. Qiao, S. Chandra, and J. Mostaghimi, "Capillary Effect during Droplet Impact on a Solid Surface," *Phys. Fluids.*, **8**, 650 (1996).

Ranade, V. V., *Computational Flow Modeling for Chemical Reactor Engineering*, Academic Press, London (2002).

Reznik, S. N., and A. L. Yarin, "Spreading of an Axisymmetric Viscous Drop Due to Gravity and Capillarity on a Dry Horizontal Wall," *Int. J. Multiphase Flows*, **28**, 1437 (2002).

Richard, D., C. Clanet, and D. Quéré, "Contact Time of a Bouncing Drop," *Nature*, **417**(6891), 811 (2002).

Richard, D., and D. Quéré, "Bouncing Water Drops," *Europhys. Lett.*, **50**(6), 769 (2000).

Rider, W. J., and D. B. Kothe, "Stretching and Tearing Interface Tracking Methods," *AIAA Paper*, 95-17171 (1995).

Rider W. J., and D. B. Kothe, "Reconstructing Volume Tracking," *J. Comput. Phys.*, **141**, 112 (1998).

Rioboo, R., M. Marengo, and C. Tropea, "Time Evaluation of Liquid Drop Impact onto Solid, Dry Surfaces," *Exp. Fluids*, **33**, 112 (2002).

Rudman, M., "Volume Tracking Methods for Interfacial Flow Calculations," *Int. J. Numer. Methods in Fluids*, **24**, 671 (1997).

Scheller, B. L., and D. W. Bousfield, "Newtonian Drop Impact with Solid Surface," *AIChE J.*, **41**(6), 1357 (1995).

Stow, C. D., and M. G. Hadfield, "An Experimental Investigation of Fluid Flow Resulting from Impact of a Water Drop with an Unyielding Dry Surface," *Proc. R. Soc. Lond. A*, **373**, 419 (1981).

Szady, M. J., and S. Sundaresan, "Effect of Boundaries on Trickle-Bed Hydrodynamics," *AIChE J.*, **37**, 1237 (1991).

Ted, M., D. C. S. Kuhn, and H. Tran, "Spread and Rebound of Liquid Droplets upon Impact on Flat Surfaces," *AIChE J.*, **43**(9), 2169 (1997).

Thoroddsen, S. T., and J. Sakakibara, "Evolution of the Fingering Pattern of an Impacting Drop," *Phys. Fluids*, **10**, 1359 (1998).

Unverdi, S. O., and G. Tryggvason, "A Front Tracking Method for Viscous, Incompressible, Multi-Fluid Flows," *J. Comput. Phys.*, **100**, 25 (1992).

Youngs, D. L., "Time-Dependent Multi-Material Flow with Large Fluid Distortion," *Numerical Methods for Fluid Dynamics*, K. W. Morton and M. J. Baines, eds., Academic Press, New York (1982).

Zhang, X., and O. A. Basaran, "Dynamic Surface Tension Effect in Impact of a Drop with a Solid Surface," *J. Colloid Interface Sci.*, **187**, 166 (1997).

Appendix: Aspects of VOF Method

Numerical aspects of the VOF method are discussed in this Appendix. Details of the geometric reconstruction scheme used to reconstruct interface position are discussed in the next section. Calculation of advected fluxes of volume fraction through the cell faces is discussed in the second section. Finally, the wall adhesion boundary condition and treatment of the gas–liquid–solid contact line on a no-slip solid surface are discussed in the last section.

Geometric interface reconstruction scheme

The geometric reconstruction scheme was used to represent the interface between immiscible fluids. This scheme is based on the piecewise linear interface calculation (PLIC). The geometric reconstruction scheme was derived from the work of Youngs (1982). Rider and Kothe (1998) generalized this scheme for structured as well as unstructured meshes. In this scheme, a straight-line segment approximates an interface within a computational

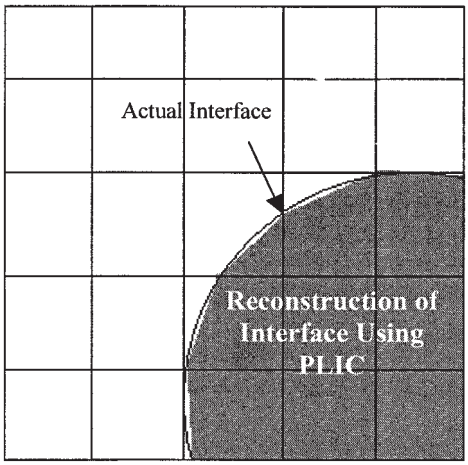

Figure A1. PLIC for calculating interface approximation and face flux.

cell (Figure A1). Note that because of linear approximation, the interface is discontinuous from cell to cell. The slope of the line segment, approximating an interface within a computational cell, is determined from the interface normal, which is calculated from the gradients of volume fraction (see Eq. 8).

The algorithm proceeds according to the following steps: (1) From the known volume fraction field, the interface normal is calculated from the gradients of volume fraction (see Eq. 8). (2) The interface position is approximated by drawing a line using the following equation:

$$\mathbf{n} \cdot \mathbf{x} + c = 0 \tag{A1}$$

where $\mathbf{n}$ is the interface normal and c is an adjustable constant. With some initial estimation for this constant c, points of intersection of this line and edges of the computational cell are obtained. A polygon is constructed from these points of intersection and those vertices of the computational cell, which lie in fluid 1. If the volume of the constructed polygon is identical to the volume fraction of fluid 1 in that cell (within stipulated tolerance), the line is assumed to represent the interface in that computational cell; if it is different, then the line constant c is adjusted using the iterative method (see Rider and Kothe, 1998 for more details).

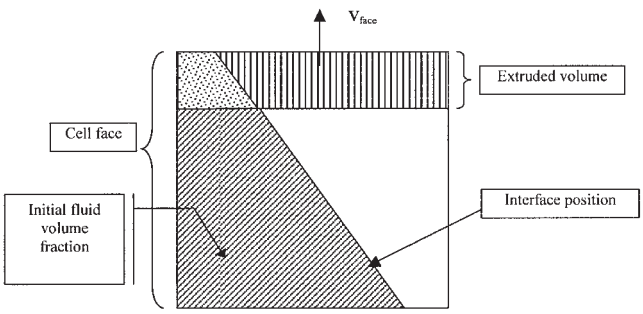

Figure A2. Advection of surface through control volume.

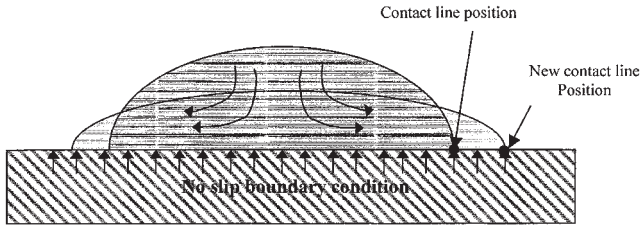

Figure A3. Movement of a contact line on the wall with no-slip boundary condition.

Advection of fluid through the control volume

Information of the reconstructed interface is used to calculate the amount of fluid advected through the cell faces. The cell face is extruded in the opposite direction to the normal velocity (see vertical shaded portion in Figure A2) to the distance normal velocity times the VOF time step (velocity field is known from the solution of momentum equations). The intersection portion (dotted area in Figure A2) of extruded volume with subsection volume (obtained in the geometric reconstruction scheme) divided by the extruded volume gives the value of face volume fraction. The face volume fraction obtained by this method was then used to calculate the effective advection fluxes of volume fraction at the cell faces. The volume fraction field is then updated by solving the usual discretized equations using effective volume fraction fluxes through cell faces.

Treatment of wall, wall adhesion, and the movement of contact line on solid surface

For fluids exhibiting a nonzero contact angle, the presence of a wall affects the surface normal and thus wall adhesion must be taken into account. The motion of a drop on the solid surface is shown schematically in Figure A3. Wall adhesion was modeled in a manner similar to that of surface tension in the case of a gas–liquid interface, except that the unit normal $\hat{\mathbf{n}}$ in this case was evaluated from the contact angle (Eq. 11). The wall adhesion boundary condition (Eq. 11) was applicable to those cells that contain a fluid interface and touch the solid surface. The unit tangent $\hat{\mathbf{t}}_w$ (in Eq. 11) is normal to the contact line and tangent to the wall. The tangent $\hat{\mathbf{t}}_w$ is directed into the fluid and computed from Eq. 8. The unit wall normal $\hat{\mathbf{n}}_w$ in Eq. 11 is directed into the wall. The contact angle was specified from the experimentally measured values.

Movement of the gas–liquid–solid contact line on the solid surface may pose unique difficulties because a no-slip boundary condition is imposed on the solid surface. However, in the present numerical implementation of the VOF model, the solid wall boundaries coincided with the cell boundaries. The no-slip boundary condition was implemented by setting the velocity at such cell boundaries (faces) to zero. The velocities at the cell center or cell faces other than those adjacent to the solid surface were not zero. Such nonzero velocities influence the volume fraction field and thus the position of the interfaces. Thus, such implementation achieves movement of the gas–liquid–solid contact line despite specifying a no-slip boundary condition at the solid surface.

Manuscript received Feb. 13, 2003, and revision received May 18, 2004.